NATIONAL AERONAUTICS AND SPACE ADMINISTRATION

Technical Report No. 32-734

Mariner Mars Absorptivity Standard

T. O. Thostesen

D. W. Lewis

JET PROPULSION LABORATORY

CALIFORNIA INSTITUTE OF TECHNOLOGY

PASADENA, CALIFORNIA

March 1, 1967

NATIONAL AERONAUTICS AND SPACE ADMINISTRATION

Technical Report No. 32-734

Mariner Mars Absorptivity Standard

T. O. Thostesen
D. W. Lewis

Approved by:

J. N. Wilson, *Manager*
Mariner Development

JET PROPULSION LABORATORY
CALIFORNIA INSTITUTE OF TECHNOLOGY
PASADENA, CALIFORNIA

March 1, 1967

TECHNICAL REPORT NO. 32-734

Prepared Under Contract No. NAS 7-100
National Aeronautics & Space Administration

CONTENTS

CONTENTS (Cont'd)

TABLES

FIGURES

FIGURES (Cont'd)

ABSTRACT

An instrument, the absorptivity standard, was used to investigate the solar absorptance of four surfaces typically used for spacecraft temperature control, the experiment being conducted as part of the *Mariner IV* spacecraft on its mission to Mars during 1964. The technique consists of measuring the temperature of a flat surface which is maintained normal to the sunlight and isolated from the thermal radiation and conduction influences of the spacecraft. The absorptivity standard includes a unique thermometer assembly that permits discrete inflight temperature measurements to within 0.2°F over a 200°F range. The seven-month flight time to Mars, the slowly changing solar intensity, and the Sun orientation of the spacecraft made the *Mariner* an ideal mission for this experiment. The test surfaces were selected on the basis of their temperature control use, ultraviolet stability, emittance, solar absorptance, and spectral sensitivity; they comprise a black paint, a zinc-oxide potassium-silicate white paint, an aluminum silicone paint, and a polished metallic aluminum. A description of this instrument and a comparison between laboratory tests and the flight data for these surfaces form the basis for this Report. An estimate of the accuracy of these measurements is also discussed, and suggestions are offered for improvements in the design of future flight experiments.

I. INTRODUCTION

The temperature of a spacecraft component is dependent on the dynamic interactions of many factors, including solar irradiation, internal power dissipation, radiative and conductive heat exchange with the surroundings, and the thermal mass of the components. These factors are, in turn, complex. Solar inputs depend on the solar intensity S, illuminated area A_p, and surface absorptance α_s to sunlight. The internal power is a function of the operational sequence of the electronics. The radiative heat exchange depends on the shape and size of the surface area (A_t), the spatial relationships to other surfaces F, the surface emissivity ϵ, and on the absorptance to incident radiant fluxes α. The conductive heat exchange is a function of the area and contact resistance of the joints, in addition to the more familiar material conductivity. As components are joined to create assemblies and, thence, the total spacecraft, the thermal interactions and interdependencies become extremely complex.

On long-flight-time missions, the problem is complicated by the change of surface properties as a function of time of exposure to the environment, as well as by changes in the environment, itself—such as the decreasing solar intensity as a spacecraft travels to Mars.

The temperature control scheme of a spacecraft is based on analysis and verified by testing in a space simulation facility. The temperature control is modified, if necessary, by an iteration between analysis and test until a satisfactory system is derived. Since the data from the space simulator tests are influenced by the idiosyncrasies of the simulator, this fact must be considered in making valid interpretations. The test temperatures reflect the finite chamber wall temperatures and the non-columnarity, non-uniformity, and spectral mismatch of the simulated solar radiation with sunlight. Some information on the effect of each of these faults can be gained during the tests in the space simulator by varying the level of the errors and by using extensive instrumentation; but the total effect can be checked only by comparison with spaceflight data.

Usually, at least one temperature transducer has a flight reading that defies the analytical and experimental predictions. In a family of spacecraft, such as the *Ranger* series, the effects of corrective changes made on each succeeding spacecraft can be observed to aid in explaining the discrepancies, and the thermal balance of later missions can be more accurately designed and predicted. In the case of a spacecraft designed for a specific mission, such as a planetary probe with a narrow launch period, errant temperatures are hard to interpret; and iteration of the thermal balance is impossible because the following spacecraft have almost entirely new design characteristics.

The *Mariner II* probe to Venus during its 1962 opposition is an excellent example of a case for which such flight data are difficult to interpret. The flight temperatures of *Mariner II* were much warmer than predicted—indeed, the telemetry indicated that some component temperatures exceeded the design limits. But while the problem was shown, the causes were masked by the multiple interactions of heat transfer between components and by the fact that the few temperature sensors that were installed were used to monitor critical temperature items, rather than to evaluate temperature control; and although postflight analysis and testing of a thermal control model spacecraft uncovered several possible causes, they could not fully explain the marked deviations from the predictions.

In the *Mariner Mars 1964* design, steps were taken to improve interpretation of temperature control data. First, the number of temperature measurements was significantly increased by a greater degree of subcommutation of the data encoder, which thereby, permitted a better coverage of the temperatures of the spacecraft. (The added measurements extended the time between consecutive readings of a given temperature transducer to a maximum of 2.8 hr; but for slowly changing temperatures, this was not considered a problem.) As a second step to aid in the evaluation of the temperature control system, an engineering experiment was flown on the *Mariner Mars* spacecraft. The instrument, the absorptivity standard[1] (Fig. 1), was designed to measure accurately the temperatures of four selected samples which were conductively and radiatively decoupled from the spacecraft. The temperature measurements were made to provide a calibration path that was independent of the other spacecraft temperature measurements. Being independent from the thermal, calibration, and electrical effects of the spacecraft, the temperatures would provide an indication of solar input. Thus, the solar heating in space, as well as that produced in the space simulator, could be directly measured, and the degradation of the surfaces vs time could be observed.

[1]It is to be recognized that the instrument measures absorptance and is not to be considered an absolute standard.

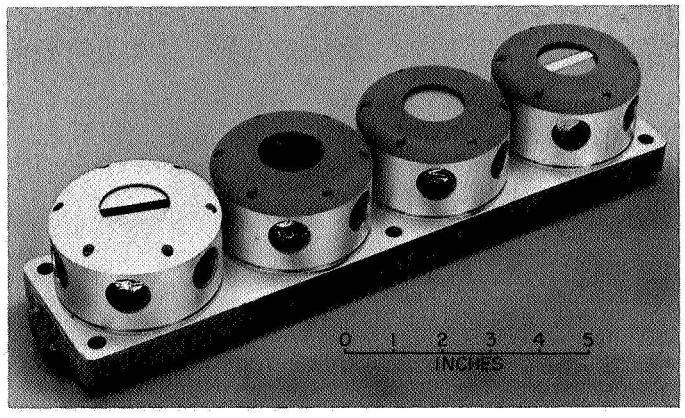

Fig. 1. *Mariner Mars* absorptivity standard instrument

II. EXPERIMENTAL METHODS FOR DETERMINING SURFACE ABSORPTANCE

A. Review of Methods

1. Spectrophotometric Method

The α_s of a surface can be computed by integration of the product of the spectral absorptance α_λ of a surface times the spectral solar model (S_λ) and dividing by the total incident energy.

$$\alpha_s = \frac{\int \alpha_\lambda S_\lambda \, d\lambda}{\int S_\lambda \, d\lambda}$$

The α_λ is determined in a laboratory by measuring the reflectance (ρ_λ) of the surface vs wavelength. The solar spectral model is based on surface and rocket measurements with appropriate corrections for the atmosphere (Ref. 1).

The α for the surface in the space simulator, similarly, can be computed by integration of spectral reflectance against the spectral intensity of the solar simulation in the chamber. The spectral model of the simulation must include the influences of the optical train on the solar simulation beam.

The accuracy of the spectrophotometric method is dependent on the uncertainties in the reflectance measurements and the solar and simulator models. The reflectance data are based on reference sources and standard detectors. As the reflectance ρ_λ increases, the errors are magnified, since $\alpha_\lambda = 1 - \rho_\lambda$. The solar spectrum is based on a limited number of ground observations with corrections to account for attenuation in the atmosphere. The ultraviolet (UV) spectrum has been observed during rocket flights above the atmosphere, but the durations are short, and scatter in the data raises questions as to the steadiness of the radiation. The simulator sources, such as mercury xenon, have large spikes in the spectrum, and if the spectral reflectance of a surface changes drastically in the vicinity of such a spike, significant errors could arise. The accuracy could be improved by narrowing the wave bandwidth of measurement, but this process is limited by the sensitivity of the detectors.

2. Electrical Equivalent Method

In the electrical equivalent approach, as in the method of the Ångström standard, the temperature of the surface in sunlight is measured. Then the sunlight is removed, and an electric heater is used to maintain this temperature value. The power dissipated by the heater is equal to the solar energy absorbed.

While the electrical equivalent system is quite simple, it would be difficult to implement in a space instrument. The method would be sensitive to geometry errors between the *Sun-on* and *Sun-off* conditions. The accuracy would be dependent on (1) the degree of duplication of temperatures caused by the Sun and maintained by the heater and (2) the accuracy of measurement of the heater power.

3. Simplified Direct Method

The simplified direct method is to base the measurement on an analytically clean situation, such as an insulated flat plate. From the measurement of the temperature and estimated values of ε, S, and heat leaks, it is possible to compute α_s.

The approach does have some serious problems: (1) The accuracy is very sensitive to conduction and radiation losses, (2) the ε and S value uncertainties are reflected in the uncertainty band of α_s, and (3) the temperature measurement must be accurate. With a good design and accurate temperature measurement, the accuracy of this method could be comparable with, or better than, laboratory spectrophotometric predictions.

B. Method Selected for Mariner Mars Experiment

The simplified direct method was chosen as the basis of the design for the absorptivity standard. The instrument measures the temperatures of four samples that are normal to the solar radiation and are conductively and radiatively isolated from the spacecraft. The selection of this approach followed from constraints imposed on the absorptivity standard.

1. Constraints

It is necessary to recognize the relative importance of this instrument in the design of the spacecraft. Although

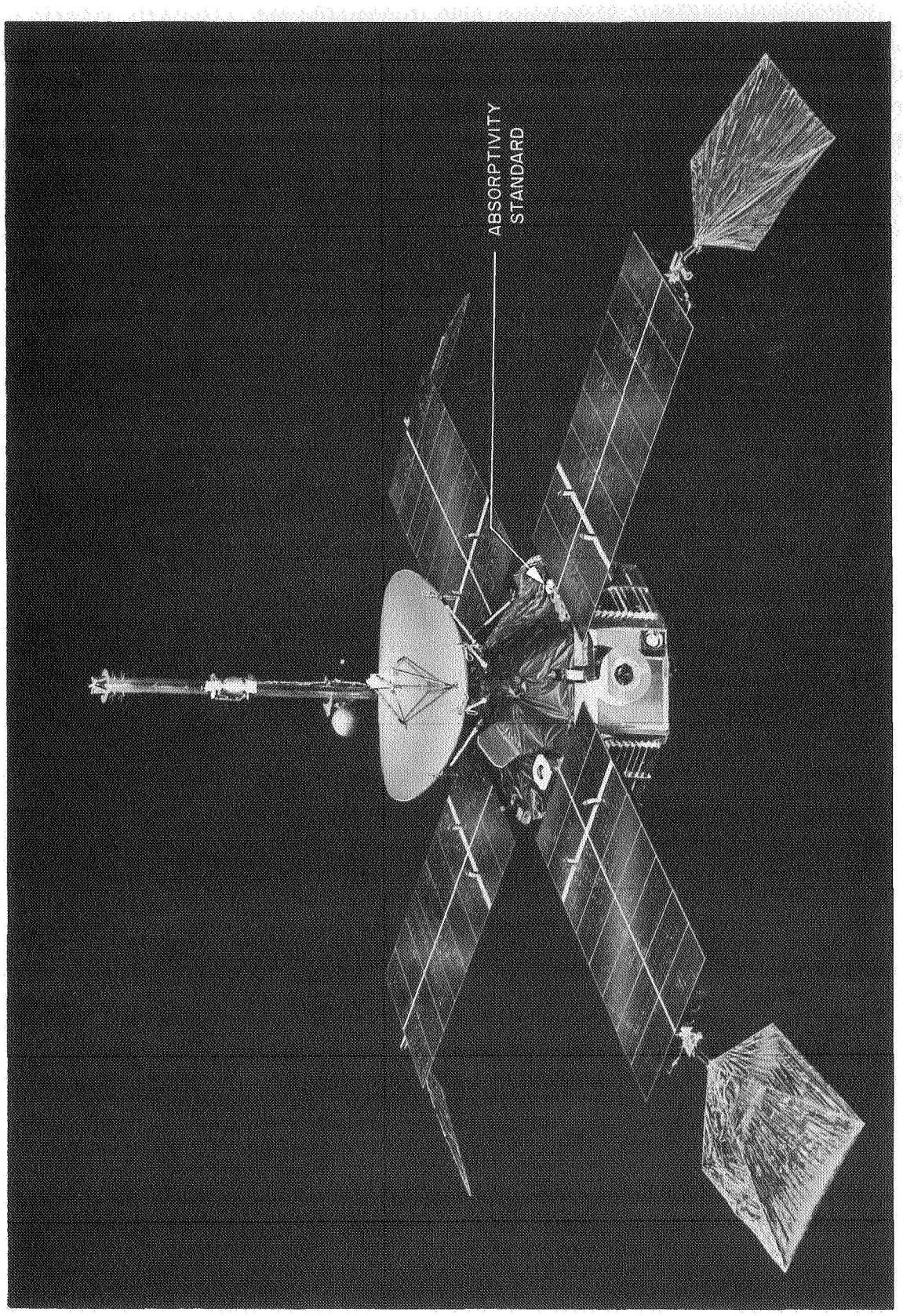

Fig. 2. *Mariner Mars* 1964 spacecraft

valuable for evaluating the performance of the temperature control system, the absorptivity standard would probably not provide any inflight information that would improve the chance of a mission success. A possible exception to this would be an observed temperature control problem in the first spacecraft before the launch of a second spacecraft. However, even in such an instance, it would be almost impossible to make adjustments on the spacecraft during the relatively short launch period.

Since the absorptivity standard experiment was of secondary importance in attaining mission success, its flight priority was low; so it logically followed that if the instrument caused conflict with weight, schedule, or manpower requirements, it would be removed from the spacecraft. Therefore, any interface with the spacecraft would be minimal; specifically, no special circuitry was to be required by the data encoder, no electrical power was to be used, the weight was to be limited to approximately one pound, and generally, its inclusion should not compromise the spacecraft design in any way. In addition, the instrument was required to meet the type approval (TA), flight acceptance (FA), and quality assurance (QA) standards required of any flight item.

2. Advantages

The *Mariner Mars* spacecraft (Fig. 2) is ideal for a surface properties experiment. The spacecraft is Sun oriented to within $\pm\frac{1}{2}$ deg angle for almost the entire $7\frac{1}{2}$ months from launch to encounter. Therefore, an instrument mounted on the sunlit side of the *Mariner* is continuously illuminated for over 3500 Sun hours [equivalent to 3500 hr at 1 AU (see Fig. 3)]. The top side of *Mariner* is relatively uncluttered, so that only 9% of the field of view of the instrument is blocked; this clear view is shown in Fig. 4, which is the view of the spacecraft reflected in a parabolic mirror (Ref. 2) that has been placed on the absorptivity standard. Each unit in the mirror grid represents a form factor of 0.001 from the surface (on which the mirror sits) to space.

Because of the increasing distance from the Sun, the temperatures decrease slowly, making possible a unique precision temperature measurement system using a step, or digital, thermometry. With the step thermometry system, the time at which a precise temperature is reached is observed, rather than a continuously varying record of temperature. This system evolved as a means to circumvent inherent inaccuracies of the typical *Mariner* temperature measurement.

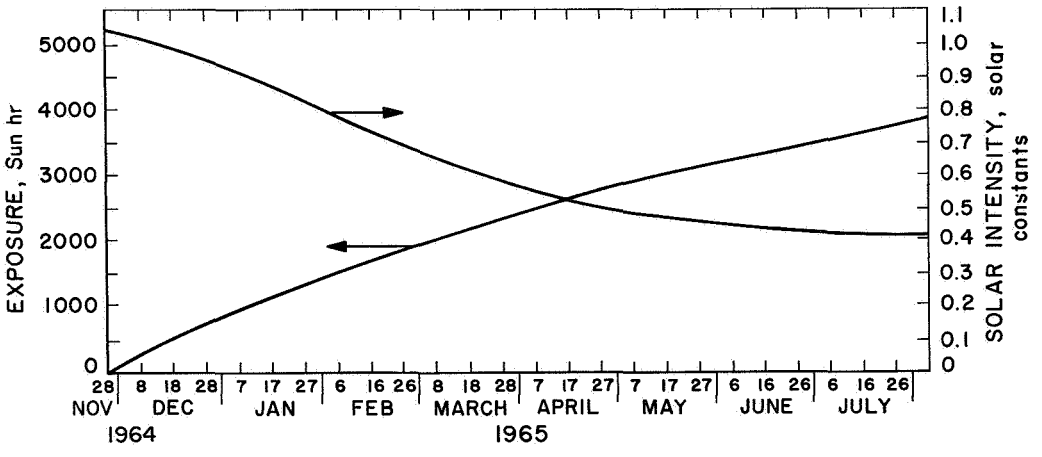

Fig. 3. *Mariner IV* solar intensity and Sun hr of exposure vs day of flight

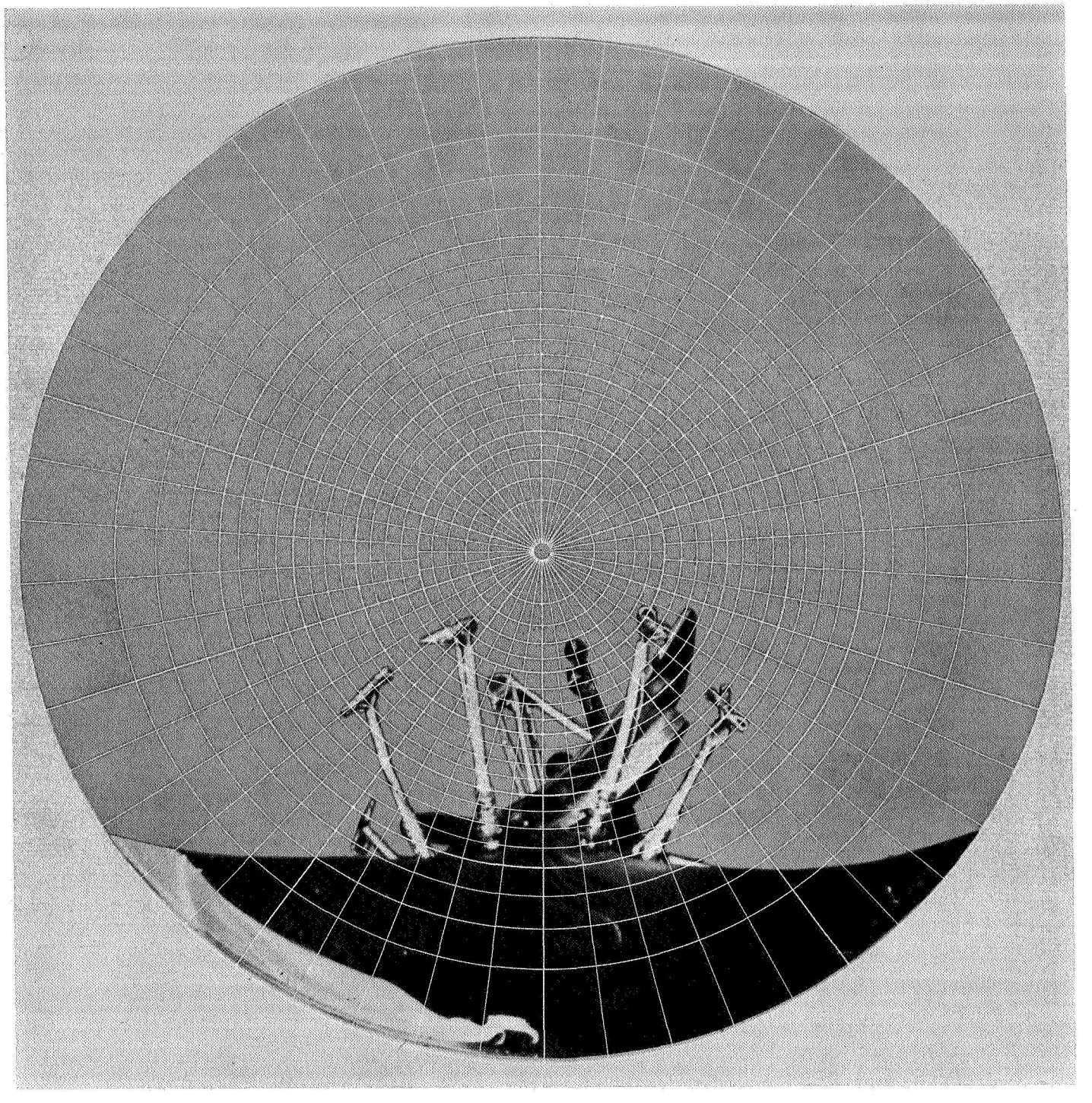

Fig. 4. Reflection in parabolic mirror used to show view of spacecraft from absorptivity standard

III. EQUIPMENT DESCRIPTION

A. Basic Geometry

It was required that the test sample surface act as an insulated flat plate normal to the solar radiation; the resulting design is shown in Fig. 1, and an individual sample assembly is shown in cross section in Fig. 5. The design reflects the attempt to isolate the sample surface from conduction and radiation heat interchange with the spacecraft and to assure the unit's surviving TA and FA testing.[2]

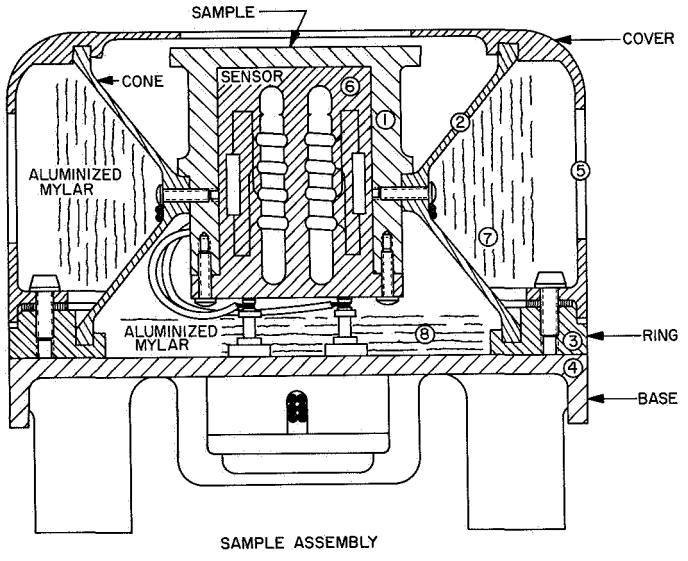

Fig. 5. Cross section of an individual sample assembly

Figure 5 shows the sample surface located on the end of a polished aluminum cylinder 1, which encloses the thermometer assembly 6. The sample cylinder is mounted in a double conical plastic support 2 which is sandwiched between the plastic cover 5 and the aluminum mounting ring 3. The cover and support are made of plastic[3], chosen for its qualities of strength at flight temperatures, low thermal conductivity, and ease of machining and casting. The cover serves to block radiation from sources other than the Sun. In addition, the lip of the cover overhangs the edge of sample surface to prevent stray sunlight from reaching the cavity between the support and the sample cylinders. The underside of the lip opposite the sample is painted black to prevent reflections. The support cone is wrapped with aluminized mylar 7 and disks of this material 8 are laid on the base to reduce radiation exchange within the assembly. The sensor lead wires are wrapped around the support structure before being attached to the terminal posts, so as to reduce conduction losses directly from the sensor. Four such sample assemblies are mounted in a row on a plastic base 4 which, in turn, is located above the upper thermal shield on the upper structural ring to provide continuous normal solar illumination. All plastic parts are coated with vacuum-deposited aluminum to give a low emissivity. To reduce sample cylinder heat leaks, the sunlit areas of the base and covers were painted to provide temperatures approximating the respective sample temperatures.

A revised support of the sample cylinder was considered and tested. The lower cone of a sample support was machined off, and the remaining portion, in which a sample cylinder was mounted, was cemented in place in a cover. The modified assembly passed TA tests, and heat leaks from the sample were reduced; but the modification was rejected because the sample cylinder could not be removed once the support and cover were joined. Redesigning to permit sample removal after assembly could not be completed within the *Mariner* time schedule.

B. Temperature Sensor Design

1. Platinum Resistance Thermostat-Switch System

The standard temperature measurements on *Mariner* were made by passing a 1-ma current through a calibrated resistance thermometer and measuring the voltage drop across the transducer. This voltage drop is converted in the data encoder into a data number (*dn*) with a digital format of 126 increments, and the information is telemetered to Earth. The inherent uncertainties of this temperature measurement system of $\pm 4°F$ made it desirable to calibrate the transducers of the absorptivity standard during flight. The sensor system initially chosen employed a platinum resistance thermometer wound on a spool, which was fitted into the cavity in the sample cylinder. Two thermostat-switches[4] were mounted in the spool to provide two inflight calibrations for the sensor to $\pm 0.3°F$. The switching temperatures and mode of operation were chosen to provide calibrations near the beginning and end of the flight, as shown

[2]JPL Specifications MC30250 and MC30251.

[3]The only plastic used was Lexan, a product of GE Chemical and Materials Dept., Pittsfield, Mass.

[4]Klixon thermostat-switches were used in this sensor system. They are manufactured by Elmwood Sensors, Inc., Providence, R.I.

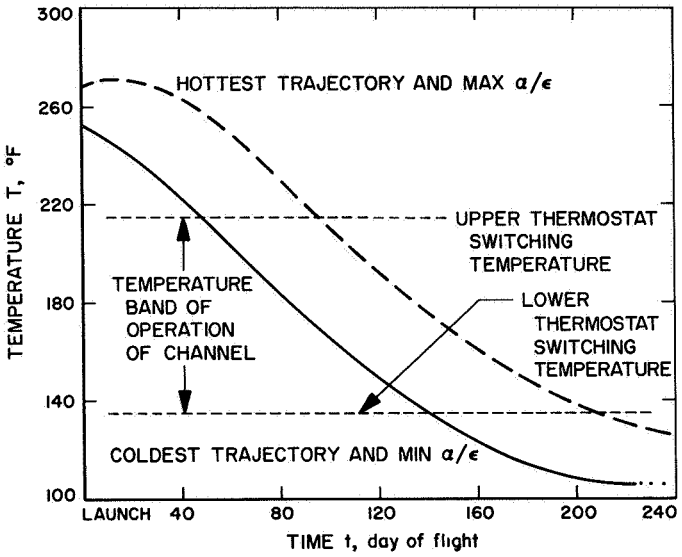

Fig. 6. Temperature vs time for black sample

in the temperature vs time plot of Fig. 6. One thermostat-switch is constructed to break contact as the temperature decreases through the switching point, which is selected to be below the minimum predicted equilibrium temperature after launch. The switch is wired to a shunt across the resistance thermometer so that the telemetry channel reads 0 *dn* until the temperature falls to the switch set point, at which time the shunt is removed and temperature data are received. As the temperature continues to fall, the telemetry gives a continuous digital history of the temperature. When the second thermostat-switch temperature is reached, the contacts close and place a shunt in the circuit, setting the channel signal at 0 *dn*. The lower switching temperature was chosen to be above the maximum expected temperature at Mars.

The thermostat-switches are off-on units that operate by the snap action of a bimetal Belleville spring. There is considerable hysteresis between the heating and cooling actuation temperatures, but the temperature at which the switch snaps when cooling, or heating, is reproducible to within 1/4°F. This accuracy, combined with the uncertainty as to the precise time at which the switch operated, provides two inflight calibrations of ±0.3°F tolerance. Since the *Mariner* data system varies only slowly, calibration checks at the beginning and end of the data would aid in its interpretation.

During a post-TA vibration test checkout, it was found that one thermostat-switch failed to operate. Examination disclosed that one end of a minute glass pushrod in the switch had chipped sufficiently to render the unit inoperative. The pushrods in other switches had chipped to lesser extents.

2. Digital Mercury Thermometer System

Because of the problem with the thermostat-switches, the temperature sensor design was reviewed. It was decided the switches could be modified by replacing the glass rod with a ceramic rod, or a different sensor system could be substituted. After comparison with the platinum resistance thermometer-thermostatic switch sensor, an alternative sensor system, which was an extension of the inflight calibration, was selected. By use of step changes in the sensor resistance, four digital, or stepping, mercury thermometers were used to signal the times at which 12 known temperatures were reached. The primary advantage was that the digital sensor was operative during the entire flight, while a thermostat-switch sensor channel might be dead for several months after launch if the flight path and tolerances were such as to give maximum temperatures. In addition, the temperature sensor was insensitive to any variations in the *Mariner* temperature measurement system. The digital sensor fitted the sample cylinder cavity and was directly compatible with the data encoder. The cost of converting to the new sensor was comparable with that of repairing the original switches.

An individual digital mercury thermometer is shown in Fig. 7. Each of the four solder rings is connected to a platinum wire that passes through the glass thermometer wall into the capillary tube. The mercury thread is used to short out resistors bridging adjacent rings. As the mercury meniscus moves past a wire, the overall sensor resistance is changed in a step fashion, signaling the time at which a specific temperature is reached. The manufacturer[5] states that the individual thermometers are accurate to within 0.1°F, are very resistant to calibration shift, and have negligible hysteresis. The gas chambers are pressurized to 200 psi with hydrogen to give resistance to 100-*g* accelerations. Because of variables in the manufacture by hand, only one of the three steps of a thermometer can be matched to within 0.1°F of its nominal value. The other two steps will be within 2°F of the nominals. All three switch points are calibrated to the nearest 0.1°F in a thermal bath against precision thermometers periodically calibrated by the National Bureau of Standards (NBS).

A typical nominal digital thermometer sensor circuit is shown in Fig. 8a. The four thermometers and 13 resistors combine to give an output signal with 12 discrete

[5]Philadelphia Scientific Glass Co., Perkasie, Pa.

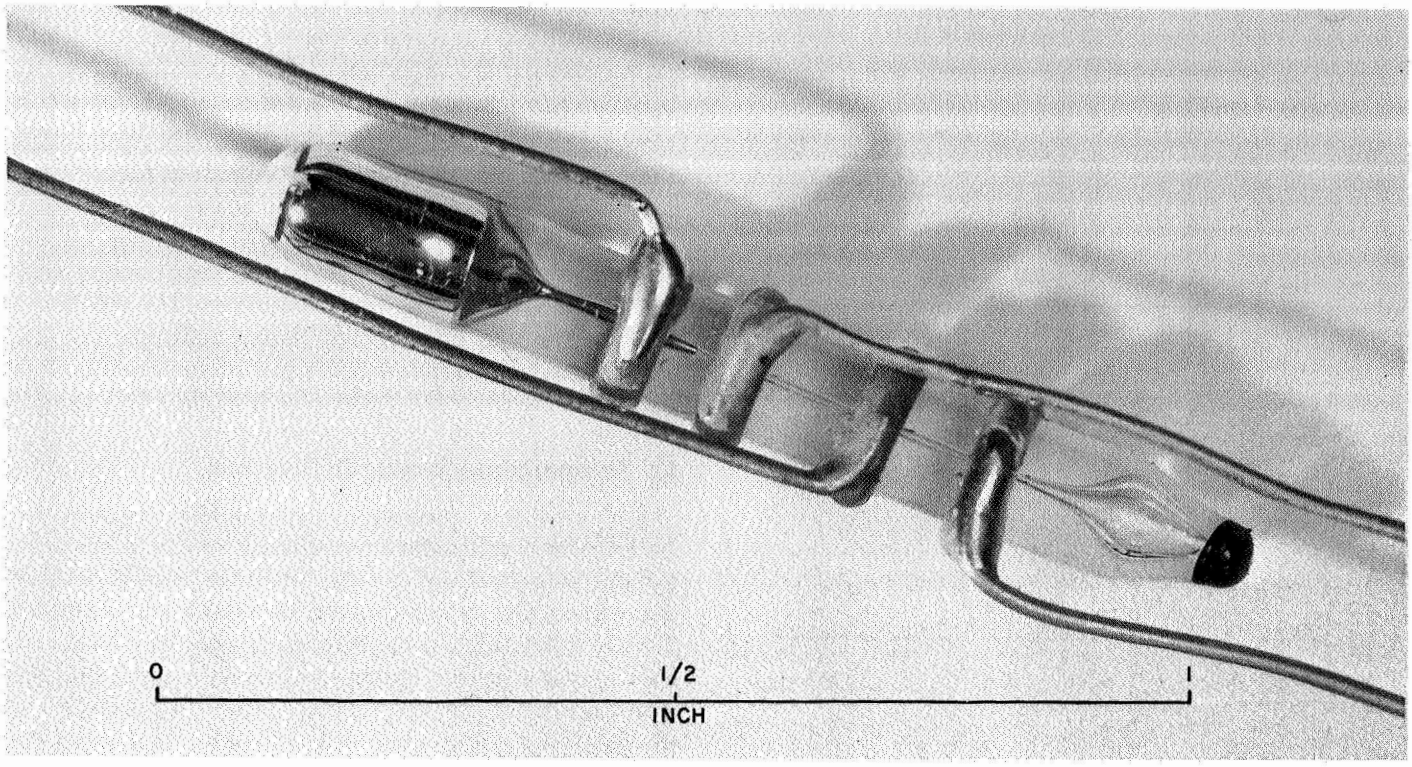

Fig. 7. Mercury stepping thermometer

steps (Fig. 8b), which is directly compatible with the data encoder. The resistance steps are a sequence of 5-, 10-, and 15-Ω increments chosen to permit identification of individual switching points in case of data encoder errors. The actual sensor output varies from about 503 to 600 Ω, rather than 500 to 600 Ω, because of the resistance of the mercury thread.

The temperatures of the steps of the sensors were selected to maximize the information returned in event of premature demise of the spacecraft. The temperature range was chosen to span the anticipated possible flight temperatures arising from surface property tolerances, the date of launch, and increasing distance from the Sun. Since the switching temperatures of an individual thermometer must be separated by at least 25°F for geometric reasons, the concentration of switching points near the launch temperatures is accomplished by overlapping the ranges of some of the thermometers. In general, the sensors each have three thermometers with overlapping ranges and a fourth thermometer that monitors lower temperatures. The polished metal sample sensor is the exception. Due to the large temperature uncertainties of the surface properties, the sensor span was extended by overlapping only the second and third thermometer ranges. The nominal switching temperatures for the sensors are shown in Fig. 9.

Figure 10 shows the 13 resistors and 4 thermometers used in a sensor, a completed sensor, and a sensor-sample cylinder assembly. The components were welded in a cordwood manner,[6] dipped in conformal coating, and potted in a glass-filled epoxy compound. The glass-filled epoxy was chosen because it gives a coefficient of thermal expansion similar to that of glass to reduce thermal stresses on the thermometers; the conformal coating yields to relieve local stress concentrations to further reduce the possibility of breakage.

3. Problems with Early Sensors

The first completed sensors were delivered to JPL with such non-nominal stepping characteristics as not stepping at expected temperatures, having resistance changes in unexpected order, and with both increasing and decreasing resistance as the temperature was varied in one direction. The symptoms were those of having

[6]Work performed at WEMS, Inc., Hawthorne, Calif., subcontractor for sensor assembly.

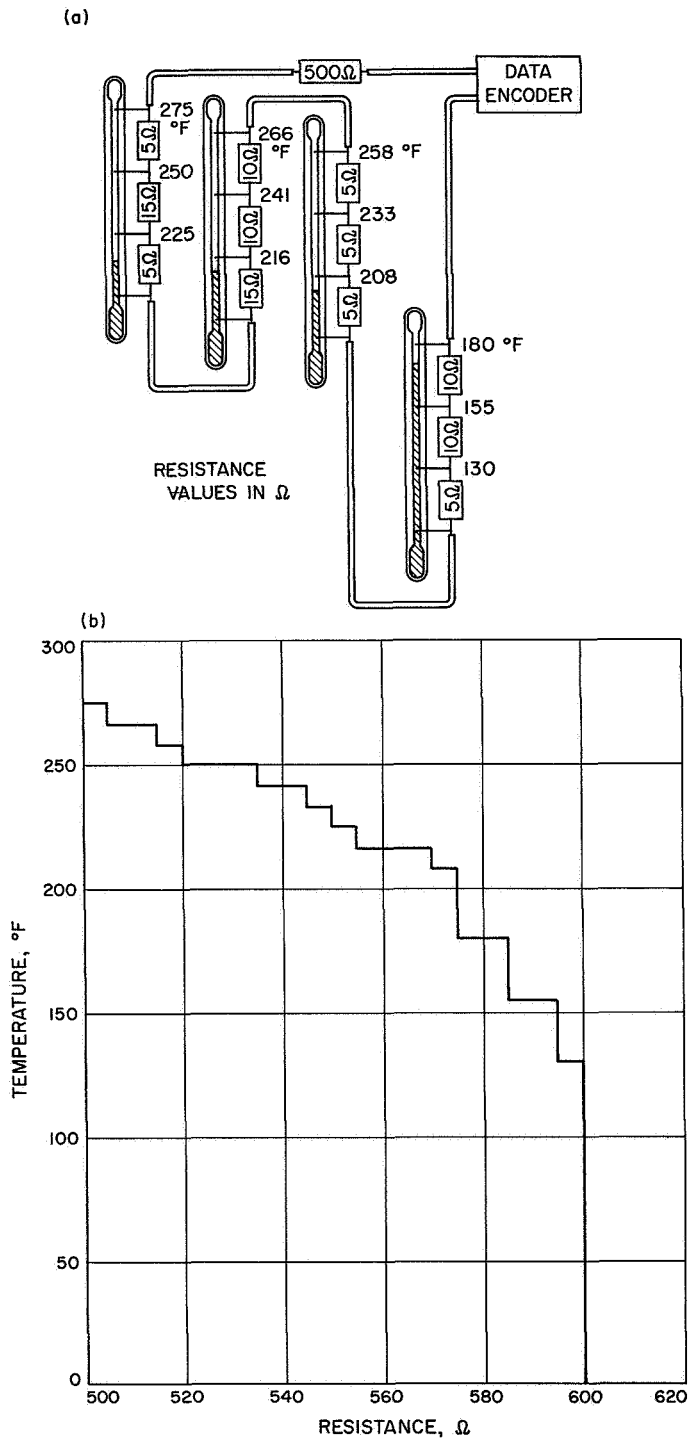

Fig. 8. Mercury step-sensor system: J-410-1676 a. Schematic of nominal digital thermometer circuit b. Stepped output signal: nominal resistance vs temperature

bubbles in the thermometer mercury threads. The problem was traced to the curing of the potting compound at 65°C for 24 hr. The mercury in the lower range thermometers (particularly the No. 4 of the white sample with switching points of 0°, 25°, and 50°F) was welling up into the gas chamber, where it is vulnerable to shocks; further, the molding die had the thermometers in a horizontal attitude during the curing cycle. The No. 4 white thermometer was redesigned to include a longer capillary above the top switch point so that the mercury would be restrained during the curing operation. The bubbles were removed by a process of heating and cooling while the sensor was spinning on a centrifuge. The creation of bubbles was also encountered during calibration at JPL. This reason for calibration shifts was encountered in flight and is discussed in the flight results of the black sample.

C. Temperature Sensor Calibration

The platinum resistance thermometer thermostatic-switch sensor calibrations were based on the calibrations by the manufacturer[7] on the platinum resistance thermometers. The calibration of the spool was extended from a water triple-point reference, using the Calendar-Van Dusen equation. After the two thermostat-switches were mounted in the spool, their temperatures at the switching points were determined by monitoring the platinum resistance thermometer. A check of a platinum resistance thermometer calibration was made at JPL. The resultant plot of resistance vs temperature paralleled the manufacturer's calibration but was displaced by 1°F. The difference is attributed to an ice reference problem at JPL.

The individual mercury digital thermometers were calibrated by the manufacturer to 0.1°F in a circulating liquid bath with a set of precision mercury thermometers, which are periodically sent to NBS for recalibration.

During sensor assembly and during the flight qualification testing, each unit was checked often for calibration shifts. The contractor for sensor assembly verified the unit operation after welding but prior to potting. After potting, the completed sensor assemblies were roughly calibrated against a set of mercury thermometers at JPL. The sensor and reference thermometer were inserted into an aluminum block, and the temperature was slowly varied to determine the sensor switching temperatures and resistance changes. This setup was used to monitor the progress in the process of eliminating bubbles and other abnormalities. Following the TA and FA qualification tests, the sensors were checked against the mercury thermometers to verify that no switching temperature had shifted.

[7]Trans-Sonics, Inc., Burlington, Mass.

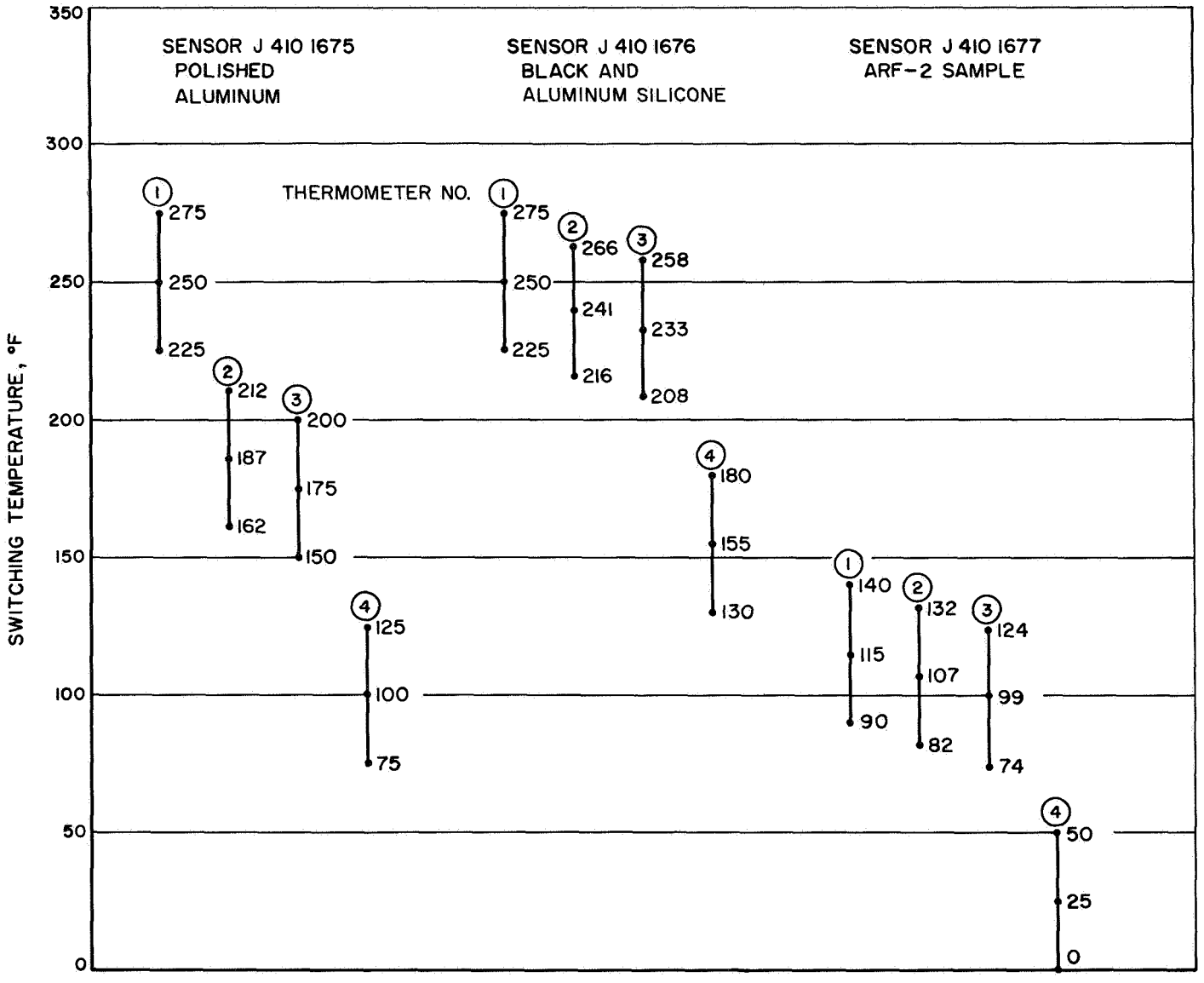

Fig. 9. Nominal sensor switching temperatures, *Mariner Mars* absorptivity standard

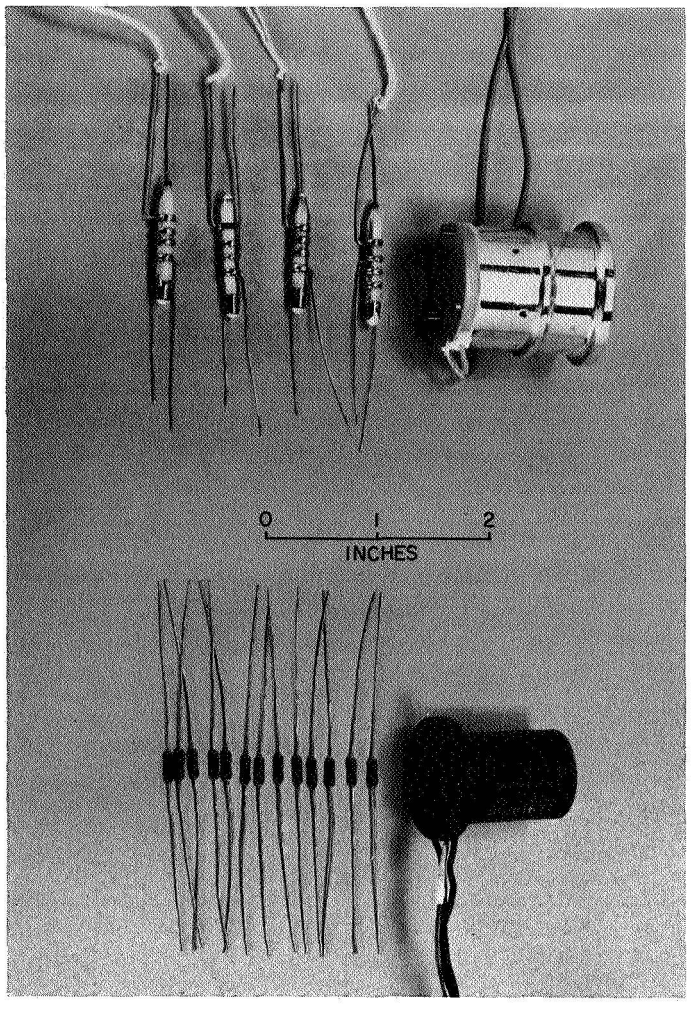

Fig. 10. Sensor components and assembly

The flight qualified sensors were calibrated for flight at the JPL Standards Laboratory with a precision platinum resistance thermometer which, in turn, had been calibrated by NBS. The sensors were inserted into an aluminum block along with the resistance thermometer. The block temperature was slowly drifted upward and downward through the sensor switch points. The difference between the switching temperatures when heating and cooling ranged from 0.2°F to 0.7°F, with a median of 0.3°F. Generally, the manufacturer's thermometer calibration fell about 0.3°F outside of the maximum or minimum, measured switch temperatures. The hysteresis noted in the calibration testing is partially due to the transient condition of the calibration and the low thermal conductivity of the potting compound. In addition, some hysteresis was found in the digital thermometers, themselves. An individual thermometer was tested in the JPL Standards Laboratory and the hysteresis of two of the switching points was found to be 0.3°F and 0.5°F, with the switching temperatures reproducible to 0.03°F. Therefore, it is felt that the actual sensor switching temperatures fall within the hysteresis band measured, with a bias toward the lower bound for this mission—since the temperatures are falling during the flight to Mars. The flight sensor calibrations are listed in Table 1.

D. Test Samples

The four sample surfaces were chosen to include a wide range of α_s/ε.The selection was also made to secure the best coating in a particular class or the most representative of the thermal control surfaces of the *Mariner Mars* spacecraft. The α_s vs ε for the four sample surfaces selected is shown in Fig. 11.

A zinc-oxide potassium-silicate paint, ARF-2,[8] was chosen to represent the white paints because of its low α_s and high ε. The laboratory measurements of the optical properties are $\alpha_s = 0.16$ and $\varepsilon = 0.86$. The ARF-2 paint was found to be very resistant to UV exposure in laboratory testing and was expected not to degrade by yellowing during the Mars mission.

[8]Also known as Z-93, a designation of the Illinois Institute of Technology Research Institute (IITRI), formerly the Armour Research Foundation (ARF).

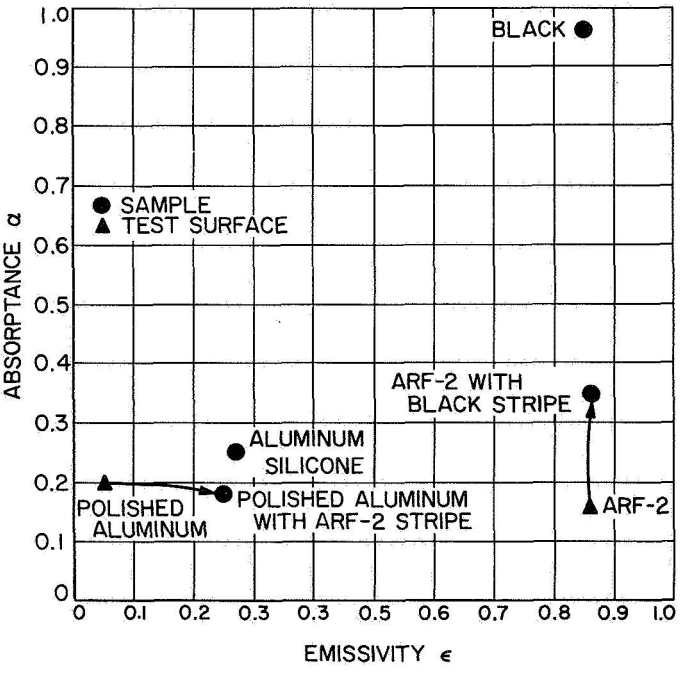

Fig. 11. Emissivity vs absorptance of absorptivity surfaces and samples

Table 1. Flight sensor calibrations

a. Channel 412, ARF-2 paint, sensor J-410-1677-5

Step temp, °F	Hysteresis, ± °F	Mfr's calib, °F	Telemetry, *dn*
139.6	0.3	139.6	4
131.7	0.1	132.0	10
123.8	0.1	123.9	22
113.5	0.1	113.4	28
108.3	0.1	108.7	47
98.0	0.2	98.1	59
92.3	0.2	92.0	65
83.1	0.3	83.7	71
77.2	0.2	77.6	90
49.7	0.3	50.0	96
25.2	0.2	25.6	109
−4.6	0.2	−4.0	121
			126

b. Channel 432, black paint, sensor J-410-1676-9

Step temp, °F	Hysteresis, ± °F	Mfr's calib, °F	Telemetry, *dn*
273.6	0.2	274.0	5
264.5	0.2	265.7	11
258.0	0.2	258.2	23
245.6	0.2	245.6	29
243.3	0.2	244.0	48
235.1	0.1	234.8	60
225.9	0.2	225.7	66
215.4	0.1	216.0	72
207.5	0.2	207.4	91
179.9	0.2	179.9	97
155.3	0.1	155.4	109
127.1	0.1	127.2	121
			129

c. Channel 413, aluminum silicone paint, sensor J-410-1676-10

Step temp, °F	Hysteresis, ± °F	Mfr's calib, °F	Telemetry, *dn*
274.6	0.2	275.0	5
264.3	0.2	265.5	11
257.7	0.2	258.4	23
252.5	0.2	252.8	30
241.5	0.2	242.5	49
229.6	0.2	230.4	61
228.2	0.2	228.2	67
217.1	0.1	217.8	73
202.2	0.1	203.0	92
179.1	0.1	179.5	97
157.1	0.1	157.0	110
132.5	0.1	132.5	122
			126

d. Channel 433, polished aluminum, sensor J-410-1675-5

Step temp, °F	Hysteresis, ± °F	Mfr's calib, °F	Telemetry, *dn*
273.1	0.2	274.9	4
248.3	0.2	249.6	10
224.0	0.2	225.2	22
211.7	0.2	211.9	28
200.0	0.1	200.2	47
188.3	0.1	188.3	60
175.6	0.1	175.4	66
159.8	0.1	159.8	72
152.4	0.1	152.5	91
125.4	0.1	125.1	97
99.3	0.1	98.8	109
74.0	0.4	73.1	121
			126

A black paint[9] was chosen for its stability and well known high α_s and high ε. The laboratory measurements of the optical properties are $\alpha_s = 0.97$ and $\varepsilon = 0.85$. The spectral response is flat with respect to wavelength, enabling the sample to serve as a basis to compare the solar simulation intensity with sunlight.

Aluminum silicone paint[10] was chosen for its gray spectral response and moderately low α_s and ε; the laboratory-measured optical properties are $\alpha_s = 0.24$ and $\varepsilon = 0.27$. Aluminum silicone paint, which is a commercial high-temperature, silvery paint used for mufflers and boiler stacks, is used on the solar vane actuators of the *Mariner Mars* spacecraft.

Originally, polished gold was chosen to represent metallic surfaces with moderate α_s and low ε, since some of the science instruments would possibly be gold plated. A problem arose when an ARF-2 stripe of 24% of the total area of the sample was added to the gold sample to lower the temperature to one compatible with the plastic. To permit accurate control of the paint stripe dimensions,

[9]Cat-a-lac black paint, 463-1-8, manufactured by the Finch Paint and Chemical Co., Torrance, Calif.

[10]UC 11659, a product of Pittsburgh Plate Glass Co.

a shallow recess was milled across the surface, and paint was laid in the depression. The copper substrate of the gold plating leached through the paint, causing a greenish cast in the ARF-2 paint. Since polished aluminum is more widely used on *Mariner Mars* for thermal shields and structural members, it was substituted for the polished gold plate. The optical properties of polished aluminum are nominally $\alpha_s = 0.17$ and $\varepsilon = 0.04$.

When the sensor design was changed, a black stripe of dimensions similar to the ARF-2 stripe on the polished aluminum was added to the ARF-2 sample surface to prevent freezing of the thermometer mercury during the later portions of the mission. The sample arrangement and configuration is shown in Fig. 12.

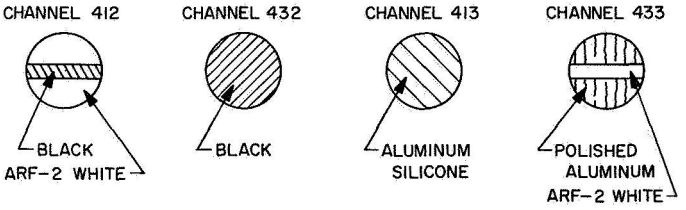

Fig. 12. Sequential arrangement of sample surfaces

IV. EARTH-BASED EXPERIMENTS

A. Conduction Tests

Modified absorptivity standard setups were tested to isolate the radiation and conduction heat losses of the sample cylinder to the cover and to the base. Knowledge of these values would be used in the error analysis (see Appendix) to aid in determining the α_s from flight data.

The primary test setup was a single absorptivity standard sample assembly set on a shortened base (Fig. 13).

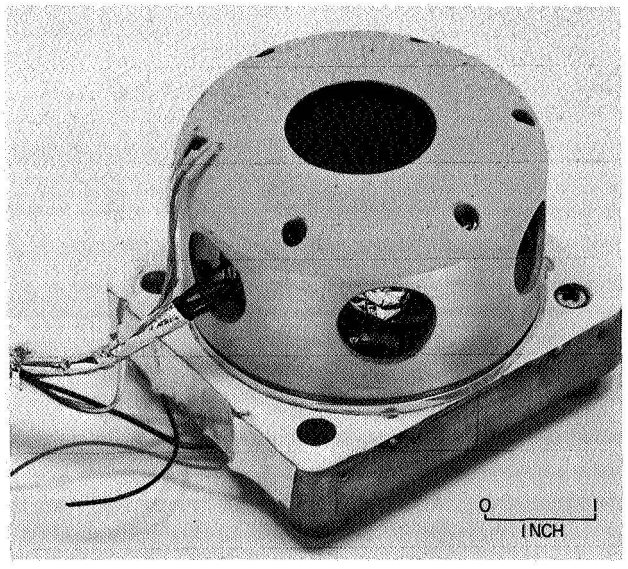

Fig. 13. Single sample test hardware

The temperature sensor was replaced by a power resistor, and the sample temperature was monitored by a thermocouple. Other thermocouples monitored the base, cover, and support temperatures. Heaters were placed on the normally sunlit areas of the cover and the base to provide simulation of the solar energy absorbed. The heater in the sample cylinder served the same function. Either the cover or base temperature was varied from a nominal case to permit computation of the radiation and conduction heat paths to the cover and the base. The first test was conducted in a bell jar with a liquid-nitrogen-cooled shroud. In this test the computed quantities for the various heat loss terms were not as expected, in that the conduction coefficients were negative and the radiation directly to space was very low. Necessary heat inputs to the sample cylinder, cover, and base to maintain a given set of temperatures were all higher than expected.

In a second test, the same single-sample setup was tested in the space simulator with solar simulation. The temperatures were cooler than flight but not as low as would be expected from the bell jar test results. This result is interpreted as indicating that the heaters did not adequately simulate the solar inputs.

Later, a test absorptivity standard (Fig. 14) was monitored, during a special test of the space simulator, to determine the effects of variations in the temperatures of

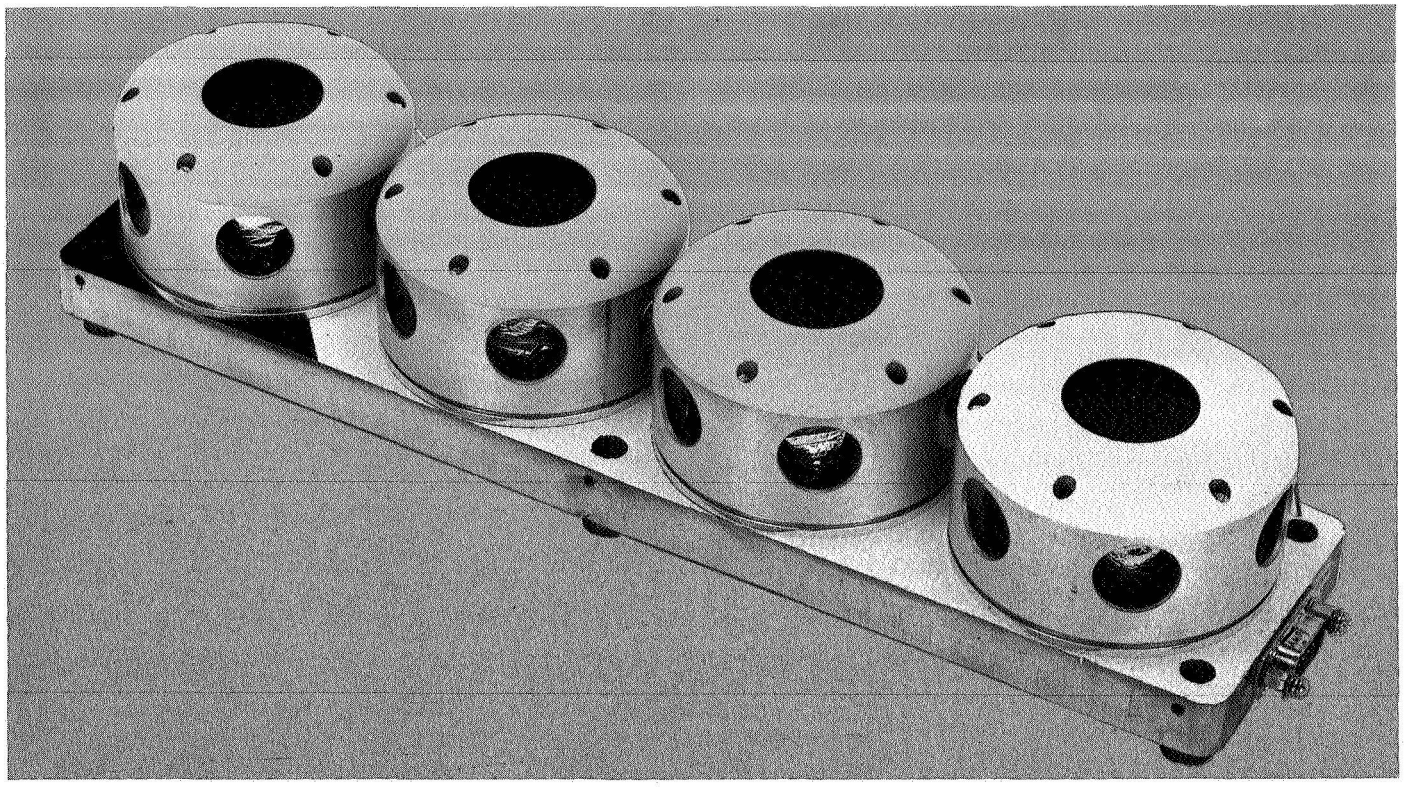

Fig. 14. Test unit used to determine effects of cover and base temperatures on sample temperature

the cover and base on the sample temperature. In this experiment, all four sample surfaces were painted with black. The cover and base paints were chosen to generate a family of temperature gradients between the sample cylinder and the cover and the base. One sample cylinder contained a heater under the paint. By adding a known quantity of heat to the sample, the heat loss could be determined more accurately. Unfortunately, the heater separated from the sample cylinder during the test, so this computational method was not completed. Analysis of heat leaks from the data of the other three samples resulted in conduction and radiation terms similar to the values found in the single-sample test apparatus. The test data did show that the radiation and conduction ties between the sample and the cover and base are significant, thereby, demonstrating that the sample surface is not a perfectly insulated flat plate.

B. Space Simulator Tests

Several tests were conducted in the 25-ft JPL Space Simulator during the evolution of the design. The temperature control model (TCM), proof test model (PTM), and flight spacecraft all carried absorptivity standards mounted in the nominal position on the upper thermal shield above Bay I. In addition, a second absorptivity standard, used to evaluate alternate designs, was placed on a solar panel next to the PTM absorptivity standard.

1. Temperature Control Model

The absorptivity standard used for the TCM test was of the original flight configuration. The sensors were composed of platinum resistance thermometers with two thermostat-switches. The cover over the white sample was painted with ARF-2. The three remaining covers were painted with black. The base was white around the white sample, and black elsewhere. The samples were ARF-2 white, black, aluminum silicone, and polished gold plate with a peripheral ring of ARF-2.

Examination of samples following the TCM testing revealed that the annular black ring on the underside of the lip of the cover had outgassed, resulting in a contamination of the surface of the sample. This problem was corrected by requiring all covers to be heated to 250°F in a vacuum chamber for 4 hr after painting.

2. Proof Test Model

The TCM absorptivity standard was used during the PTM systems test. After this test, it was found that the plastic base had so warped that the instrument could

not later be remounted on the spacecraft. Testing showed that this was the result of the plastic softening at about 270°F. To lower the base temperatures, the entire top surface of the base was painted white.

An absorptivity standard with digital thermometer sensors, a white-painted base, an ARF-2 white sample with an annular black control ring (to raise the temperature), a black sample, an aluminum silicone sample, and a polished aluminum sample with an ARF-2 annular control ring was used for the PTM thermal test. The data from the digital thermometer sensors were marginal, since the telemetry signals indicate temperature range rather than a specific value, similar to the digital format of the spacecraft telemetry but with a much poorer resolution. To give adequate comparison of simulator results with flight data, more precise data were required; therefore, thermocouples were inserted into sensors fabricated subsequent to this test. The thermocouple leads were to be removed following the space simulator tests. If a thermocouple were broken prior to testing, a thermocoupled tab was inserted between the sensor and the sample cylinder.

During the test, it was noticed that the paint on the three black covers on the PTM unit was blistered and cracked. After completion of the test, blisters were lifted off and evidence of melting of the substrate of plastic under the paint was found. To prevent recurrence of blistering, the cover paint on the three affected samples was changed from black to a PV100-based gray paint, which would lower the temperature. It was noticed that the white cover was slightly discolored on the inboard side, probably due to outgassing of the upper thermal shield. The white-painted base, although warped, probably from heating of the base while restrained by the mounting screws, could be remounted on the spacecraft.

In addition to the flight-type absorptivity standard on the spacecraft during the PTM thermal test, a special instrument with four variations of the polished aluminum sample with white control paint was placed on a solar panel (Fig. 15). The unit was used to evaluate (1) the design change of replacing the white ring by a white stripe on the polished aluminum sample surface, (2) the change from a recessed sample to a mounting on which the sample surface is flush with the cover, and (3) the removal of the lower cone of the sample support. The covers were painted black, and the base was painted white. The temperatures were monitored by platinum resistance thermometers from the thermostat-switch sensor design.

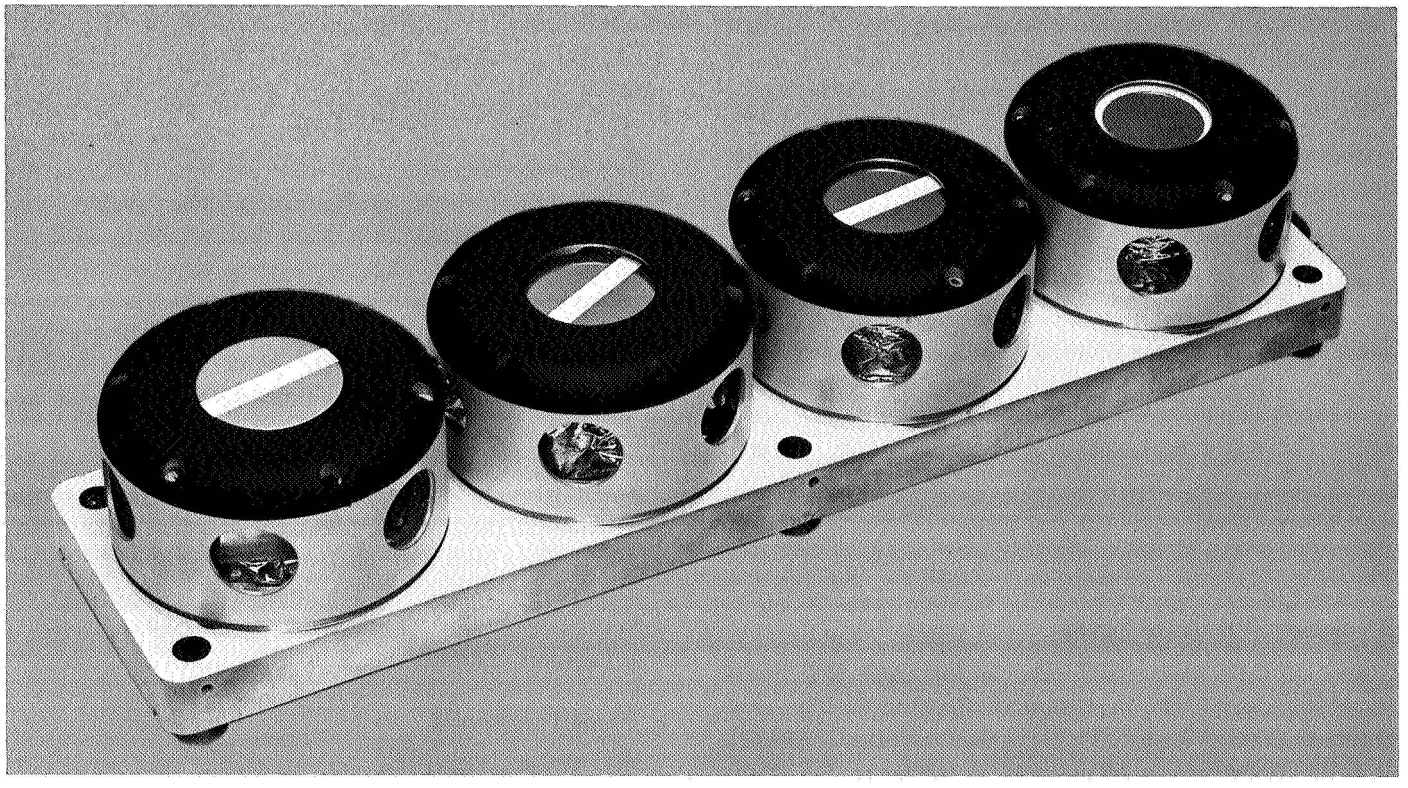

Fig. 15. Test unit with four variations of polished aluminum samples with white control stripe

The first sample was identical to the polished aluminum sample of the PTM absorptivity standard and served as a basis of comparison for the other three sample assemblies. The second sample had a white stripe in place of a white annular ring (a stripe is easier to mask when painting and would be less influenced by the cover lip overhang; also, the stripe was to be flown and the relative performance was desired). The third sample was to evaluate the effect of removal of the lower cone of the sample support as an aid in isolating the sample. The sample cylinder, with white stripe, was mounted in the abbreviated support, which was then bonded to the cover. The fourth sample cylinder was raised in its sample support so that the sample surface was flush with the enlarged hole in the cover. This was to evaluate the problems arising from sunlight entering the cavity between the sample cylinder, sample support, and cover.

Sample 1 with the white control ring ran about 40°F cooler than the equivalent sample on the PTM because of the lower solar simulator intensity on the solar panel. Sample 2 with the white stripe ran about 6°F warmer than the sample with the ring. The removal of the lower cone of the sample 3 support resulted in a 22°F temperature increase over sample 2. Mounting the sample surface flush with the cover on sample 4 had little effect.

The data demonstrated that removal of the lower support cone did significantly reduce heat leaks to the base. This concept also passed TA vibrational testing. The neutral effect of flush mounting showed that the assembly could be redesigned to permit removal of the sample cylinder non-destructively without adverse effects. Limited time prevented the system being redesigned, and modification of the present support was ruled out, since a sample surface could not be replaced, once a support was cemented in place.

3. *MC-2*

The *MC-2* was the first flight Mars mission spacecraft tested in the space simulator. The *MC-2* unit absorptivity standard, C-105, was on the spacecraft during the *MC-2* systems test, with the data being returned through the spacecraft telemetry channels only. This method proved unsatisfactory since for an accurate check of the temperatures the simulation intensity would have to be fluctuated slowly and carefully. This problem had been recognized during the PTM test and later sensors included thermocouples. These thermocouples were to be removed following final simulation testing. Between the systems and thermal testing, the C-105 was removed from the spacecraft and tab thermocouples were installed on all four sensors, resulting in a duplication of thermocouples on the aluminum silicone sample, since this sensor already had an internal thermocouple. All five thermocouples were read by the test instrumentation. The internal thermocouple agreed to within 3°F with the sample tab thermocouple.

At the time the unit was disassembled for insertion of the tabs, it was noted that the sample surfaces were discolored where they were exposed to the simulator and were clean where protected by the cover. The most reasonable source of contamination seemed to be the upper thermal shield.

4. *MC-3*

During the environmental testing, the *MC-3* absorptivity standard, C-106, sample temperatures were monitored by one tab and three internal thermocouples. During the systems test, the equilibrium temperatures at four light intensities were measured. During the thermal test, only Earth and Mars intensities were used. It was found that the thermal test results were from 9 to 17°F higher than in the systems test. The discrepancy might be explained partially by an instrumentation problem during the thermal test. Nevertheless, the thermal test results agreed with the average of the temperatures in the other simulator tests, suggesting that there was some variation of solar simulation intensity between the two tests; the intensity during the TCM test agreed more closely with other tests.

5. *MC-4*

The *MC-4* flight absorptivity standard, C-107, was tested in the space simulator during the *MC-4* spacecraft systems test. Due to a simulator vacuum system failure, the unit was lightly sprayed with diffusion pump oil. Therefore, C-107 was removed, disassembled, and cleaned—including replacement of the white cover and repainting the sample surfaces. At this time, the flight sensors, which previously had been unavailable, were substituted into the units. The rejuvenated instrument was magnetically mapped and resubmitted for quality assurance.

The temperatures during the subsequent *MC-4* systems test were from 13 to 23°F higher than those measured before the simulator outage.

6. *MC-5*

The *MC-5* flight spare absorptivity standard, C-110, was flight qualified in the space simulator during the *MC-4* thermal test.

V. FLIGHT EXPERIMENT

A. Review of Instrument Design Flown

The absorptivity standard is designed to approximate an insulated flat plate, normal to the solar radiation. The sample surface is located on one end of a polished aluminum cylinder, into which the temperature sensor is inserted. The sample cylinder is mounted in a plastic support and is radiatively isolated from the surroundings by a plastic cover and aluminized Mylar shielding. The four samples are mounted in a row on a plastic base.

The four samples, which were chosen on the basis of being representative of the different classes of surface properties, are: ARF-2 white paint with a black paint stripe, black paint, aluminum silicone paint, and polished aluminum with an ARF-2 stripe.

The sample temperatures are monitored through the spacecraft thermal telemetry system. A step change of several *dn* in the telemetry signals when a specific temperature is reached. Sensor calibration follows FA vibration tests, to an accuracy of 0.2°F. The *Mariner IV* absorptivity standard sensor calibrations are listed in Table 1. The hysteresis of each calibration point is indicated, as is the manufacturer's initial calibration.

B. Qualification of Flight Units

The flight absorptivity standards were qualified for the mission by being subjected to QA inspections, assembled and FA tested in conformance with JPL Specification MCO-31543-ETS-A, mapped for magnetic fields, and the observation of the unit performance during the flight spacecraft systems and thermal environment tests.

The component parts were inspected, on receipt, for dimensional conformance to the drawings; critical dimensions, such as the diameter of the central hole of the cover, were measured by the JPL inspection department to determine exact size. The painted sample surfaces were applied in the JPL thermal control paint shop subject to the standard specifications, techniques, and QA inspections. Test specimens were prepared at the same time as the sample surfaces so that the surface properties could be measured. Some of these test specimens were placed in the space simulator during a spacecraft test and later tested for changes in surface properties. Some of the ARF-2 white paint test specimens were subjected to prolonged UV exposure to determine degradation rates.

The temperature sensors were roughly calibrated prior to FA vibration testing. Following the shake tests, the sensors were checked for calibration shifts; if no changes were discovered, the qualified sensors were flight calibrated in the JPL Standards Laboratory. The calibrated sensors were then assembled into the flight absorptivity standard, which was then magnetically mapped, and submitted to QA as flight qualified hardware.

Usually, a system or instrument must go through FA as a unit and cannot be disassembled following FA testing without requalification being required. However, in the case of the absorptivity standard, since the sensors had to be removed from their assemblies after FA vibration testing for final calibrations, and since there was the desire to minimize handling to protect the surfaces, the guidelines were waived. Only the sensors were subjected to FA testing. Once the sensors were calibrated and assembled into the flight unit, the qualified absorptivity standard was submitted to QA. From this point on, no further work was permitted on the instrument. Therefore, sample surfaces were not cleaned or replaced after the space simulator tests.

The environmental chamber tests were considered part of the FA testing. The data through the spacecraft telemetry verified operation, and thermocouple data permitted comparison with flight data for evaluation of the space simulator.

C. Flight Data

1. Prelaunch Activities

The data from the absorptivity standard began with the tests in the space simulator. The thermocouple data for the four flight instruments during the systems and thermal tests are listed in Table 4. It is seen that the temperatures of all the samples with a given surface treatment under supposedly identical conditions were generally reproducible but that there were a few exceptions. For example, the sample temperatures were 15°F hotter during the *MC-2* thermal test than the *MC-2* systems test. Similarly, the C-107 unit ran 10 to 20°F warmer after it was rejuvenated following the vacuum failure in the *MC-4* systems test. These data suggested that the simulator environment varied from test to test.

The data obtained during prelaunch checkouts did not provide much opportunity of verifying the operation of

Table 2. Thermocouple data from systems and thermal tests

Unit	Test	Steady-state sample temperature, °F															
		White				Black				Al silicone				Polished Al			
		Simulated solar radiation intensity, w/ft^2															
		134	100	51	30	134	100	51	30	134	100	51	30	134	100	51	30
C-105	MC-2 Thermal 1	169	—	45	—	271	—	123	—	258 (255)[a]	—	109 (112)[a]	—	261	—	114	—
C-105	MC-2 Thermal 2	171	—	—	—	274	—	—	—	260 (257)[a]	—	—	—	263	—	—	—
C-106	MC-3 Systems	163	124	43	−5	263	216	115	50	242	197	95	39	249	205	105	44
C-106	MC-3 Thermal	174	—	52	—	280	—	128	—	BAD	—	BAD	—	266	—	116	—
C-107	MC-4 Systems	161	—	—	—	264	—	—	—	244	—	—	—	241	—	—	—
C-107	MC-4 Systems	174	—	39	−9	287	—	122	58	256	—	99	39	258	—	100	30
C-110	MC-4 Thermal	175	—	42	—	277	—	120	—	251	—	103	—	254	—	106	—

[a]Thermocouple internal to sensor.

the instrument. The normal indoor ambient air temperatures were included only within the sensor range of the ARF-2 sample. If the ambient increased to 75°F, one step was seen in the polished aluminum sample. The black and aluminum samples remained dormant.

2. *Mariner III*

The polished aluminum sensor on the *MC-2* spacecraft, C-104, was found to have an intermittent break in the 75°F switch point circuitry during systems testing at Cape Kennedy. Therefore, the C-104 unit was replaced by the C-106 unit from *MC-4*, and the flight spare, C-110, was assigned to *MC-4*. The C-106 unit was launched on the *Mariner III* (*MC-2*) spacecraft on November 5, 1964. The shroud failed to separate from the spacecraft, causing the mission to be unsuccessful. The data received from the absorptivity standard verified that the temperature sensor system was operating properly but was uninterpretable for determining α_s.

3. *Mariner IV*

The *Mariner IV (MC-3)* spacecraft was successfully launched November 28, 1964. Data were received from launch until October 1, 1965, when the telemetry stream was terminated. These data are tabulated in Table 5. The flight data can be separated into three groupings: post launch, midcourse maneuver, and interplanetary cruise.

Following launch from Cape Kennedy, the absorptivity standard sample temperatures were in a state of flux, going from ambient pre-launch shroud cavity temperatures to steady-state cruise temperatures. The rate at which the temperatures increased was an indication of the α_s of the individual samples; the higher the α_s, the greater the heating rate. Therefore, the black sample would respond the most rapidly, followed by the white, aluminum silicone, and polished aluminum samples. The data showed questionable characteristics in that the channel assigned to the black sample, channel 413, reacted the slowest, and the channel assigned to the aluminum silicone sample, channel 432, reacted the quickest. The white and polished aluminum sample rates seemed reasonable. All *dn* values observed were nominal.

Seven days after launch, the spacecraft was pitched 39.16 deg off the Sun–spacecraft line for one hour during the midcourse maneuver. The absorptivity standard remained in the sunlight, but the intensity was reduced by 22% because of oblique illumination. Following spacecraft reacquisition of the Sun, the sample temperature rose back to pre-maneuver values. The temperature

Table 3. Flight data from *Mariner IV*

a. Post-launch transient

Day 333, 334 Time, GMT	Data from sample channel, *dn*			
	412, White	432, Black	413, Al silicone	433, Polished Al
15:41:17	97	126	126	126
16:23:17	90	110	126	122
17:26:41	59	66	122	97
18:06:35	28	48	110	72
18:50:41	22	29	98	66
19:32:41	22	29	92	60
20:14:30	10	23	92	60
20:56:41	↓	↓	73	47
21:38:41			↓	47
22:20:41				29
23:02:41				↓
23:44:41			↓	
00:26:41			73	
01:08:41			67	
01:50:41			67	
02:21:41	↓	↓	61	↓
03:14:41	10	23	61	29

b. Midcourse transient

Day 340 Time, GMT	Data from sample channel, *dn*				Ref. operation time, GMT
	412, White	432, Black	413, Al silicone	433, Polished Al	
15:17:55	4	23	61	22	
15:31:55	4	23	↓	22	Pitch @ 15:25:08
15:45:55	10	29	↓	22	
15:59:55	↓	48	61	28	Roll @ 15:47:10
16:13:55	↓	60	67	↓	Fire motor 16:09
16:53:55	↓	48	73	↓	← Start Sun acquis. & Mode II data 16:15:11 └ Sun acquired 16:21:07
17:35:16	↓	29	67	↓	
18:17:15	10	29	61	↓	
18:59:15	4	29	61	28	
19:41:16	4	23	61	22	

Table 3. (Cont'd)

c. Interplanetary cruise

Day of yr	Date, 1964–65	Data from sample channel, *dn*				GMT		Distance from Sun R, 10^9 km
		412, White	432, Black	413, Al silicone	433, Polished Al	Time of previous *dn*	Time of change	
333	11-28	10	23	61	29	—	—	Launch, 0.14756
336	12-1	4	23		29	01:25:12	02:04:41	0.14776
337	12-2		23		22	11:00:41	11:45:42	0.14788
345	12-10		29			04:28:09	05:13:10	0.14887
01	1-1		48			14:50:55	15:32:55	0.15483
04	1-4		60	61		05:12:02	08:00:11	0.15578
05	1-5	4		67		03:43:46	06:31:46	0.15614
06	1-6	10		67		18:47:25	21:35:25	0.15677
09	1-9		60	73		14:07:53	16:55:53	0.15786
11	1-11		66			19:12:27	— [a]	
12	1-12				22	—	06:24:27 [a]	0.15932
15	1-15				28	18:32:55	—	
16	1-16	10				—	05:44:55	0.16062
21	1-21	22	66			03:11:29	05:59:29	0.16294
22	1-22		72			21:12:45	—	0.16376
23	1-23				28	—	00:00:45	
23	1-23			73	47	02:57:09	05:45:09	0.16388
27	1-27	22		92		04:56:27	07:44:28	0.16579
32	2-1	28	72			13:36:	16:24:	0.16845
33	2-2		91			23:13:01	—	
34	2-3				47	—	02:01:10	0.16921
36	2-5			92	60	04:33:39	07:21:39	0.17029
38	2-7			98		15:20:56	—	
39	2-8		91			—	02:32:56	0.17163
39	2-8		97			16:25:24	— [a]	0.17208
40	2-9		97			—	03:37:25 [a]	0.17229
44	2-13	28	110			10:24:54	13:12:54	0.17459
46	2-15	47			60	07:12:57	10:00:57	0.17555
50	2-19				66	14:58:25	— [a]	0.17786
51	2-20	47	110	98	66	—	02:10:27 [a]	0.17806

[a]Data missing during this period because Johannesburg tracking station was used for *Ranger* tracking.

Table 3c. (Cont'd)

Day of yr	Date, 1965	Data from sample channel, *dn*				GMT		Distance from Sun R, 10^6 km
		412, White	432, Black	413, Al silicone	433, Polished Al	Time of previous *dn*	Time of change	
54	2-23	59	110	98	66	08:25:23	11:13:25	0.17979
61	3-2	↓	↓	110	66	00:01:46	02:49:46	0.18337
66	3-7	↓	110	↓	72	17:14:57	20:02:58	0.18642
68	3-9	↓	122	↓	↓	22:18:40	—	—
69	3-10	59	↓	↓	↓	—	01:06:41	0.18755
69	3-10	66	↓	↓	↓	15:05:53	— [a]	0.18789
70	3-11	66	↓	↓	↓	—	02:17:56 [a]	0.18813
77	3-18	72	↓	↓	↓	13:30:26	— [a]	0.19203
78	3-19	↓	↓	↓	72	—	00:42:28 [a]	0.19226
85	3-26	↓	↓	110	91	06:28:14	09:16:14	0.19546
89	3-30	72	↓	122	↓	11:15:42	14:03:42	0.19808
94	4-4	90	122	↓	↓	14:19:42	17:07:42	0.20051
103	4-13	90	126	↓	↓	16:45:18	22:21:18	0.20490
105	4-15	96	↓	122	↓	13:32:35	16:20:35	0.20565
131	5-11	↓	↓	126	91	02:55:15	05:43:15	0.21622
137	5-17	96	↓	↓	103	12:56:41	15:44:41	0.21854
204	7-23	109	↓	↓	↓	10:13:58	19:35:05	0.23349
256	9-13	96	126	126	103	06:13:48	09:01:49	0.23465

[a] Data missing during this period because Johannesburg tracking station was used for *Ranger* tracking.

history while the spacecraft was pitched away from the Sun-line indicates the relative emissivity of the samples; samples with higher emissivities cooled more rapidly, while the transient period following reacquisition again indicates the relative magnitudes of the solar absorptances. Contrary to the expected behavior of the aluminum silicone sample, again, channel 432 responded the most rapidly. All *dn* values for the data observed during the midcourse transient were nominal.

Interplanetary cruise is a pseudo steady state, during which the temperatures slowly decrease as the spacecraft–Sun distance increases. The trajectory aphelion fell on August 26, 1965, and thereafter, the temperatures began to increase.

The first cruise mode activity was seen on day 336 when the ARF-2 white paint sample, channel 412, stepped from 10 to 4 *dn*, signaling that the sample had warmed since launch, probably due to degradation of the ARF-2. The polished aluminum sample sensor stepped from 29 to 22 *dn* the following day. This increase in temperature verified the degradation of the ARF-2 since this sample has an ARF-2 control stripe.

The next three steps were in channel 432. The two closely spaced steps on days 01 and 04, 1965, verified that channel 432 was indeed the black sample and that channel 413 was the aluminum silicone sample. It is believed that these two channels were reversed from the nominal channel assignments due to the cabling harness on this absorptivity standard being fabricated to an obsolete print. Since the reversal was easily identified, no problem in interpretation of the data resulted. The other two channels were correct as some verifying activity was observed during the pre-launch checkouts. The first step of channel 413 was seen on day 05, 1965.

The *Mariner IV* cruise data are discussed and plotted by sample in the following sections. The predicted temperature history of insulated flat plates with the nominal laboratory-measured sample properties is also plotted for comparison. In addition, the degradation of the surface properties in the space environment is indicated by a plot of the ratio of α_{s_i} the α_s at a given data point, to α_{s_0}, the α_s at the first observed switch point. The ratio of $\alpha_{s_i} / \alpha_{s_0}$ is calculated by use of the sensor calibrations and the spacecraft–Sun distance found in the *Mariner IV* trajectory tables. The thermal balance of a sample surface can be written (terms defined on page 31) as:

$$SA_p\alpha_s = \sigma\varepsilon A_t T_s^4 + Q_L \tag{1}$$

From Eq. (1), α_s is found to be

$$\alpha_s = \frac{\sigma\varepsilon A_t T_s^4}{SA_p} + \frac{Q_L}{SA_p} \tag{2}$$

The ratio of α_s at times a and b is

$$\frac{\alpha_{s_b}}{\alpha_{s_a}} = \frac{S_a}{S_b}\left(\frac{\sigma\varepsilon A_t T_b^4 + Q_{L_b}}{\sigma\varepsilon A_t T_a^4 + Q_{L_a}}\right) = \frac{S_a}{S_b}\left(\frac{T_b^4 + \dfrac{Q_{L_b}}{\sigma\varepsilon A_t}}{T_a^4 + \dfrac{Q_{L_a}}{\sigma\varepsilon A_t}}\right) \tag{3}$$

From the inverse square law, the ratio of the solar intensities is

$$\frac{S_a}{S_b} = \left(\frac{R_b}{R_a}\right)^2 \tag{4}$$

where R is the distance from the Sun.

By the substitution of Eq. (4) into (3)

$$\frac{\alpha_{s_b}}{\alpha_{s_a}} = \left(\frac{R_b}{R_a}\right)^2 \left(\frac{T_b^4 + \dfrac{Q_{L_b}}{\sigma\varepsilon A_t}}{T_a^4 + \dfrac{Q_{L_a}}{\sigma\varepsilon A_t}}\right) \tag{5}$$

If $Q_L = 0$, or is completely a function of radiation heat transfer and is, therefore, Sun dependent, Eq. (5) reduces to

$$\frac{\alpha_{s_b}}{\alpha_{s_a}} = \left(\frac{R_b}{R_a}\right)^2 \left(\frac{T_b}{T_a}\right)^4 \tag{6}$$

The opposite extreme is the case when Q_L is a constant, not varying with sample temperature. Since $T_b < T_a$, a positive Q_L will result in a larger α_b/α_a than calculated from Eq. (6), and a negative Q_L will give a smaller ratio. If Q_L is due to conduction only, the effect on $\alpha_{s_b}/\alpha_{s_a}$ is less than for constant Q_L. The effect of degradation of the paints on the covers and base between times a and b is to reduce the temperature gradient, and thereby Q_L, resulting in a larger $\alpha_{s_b}/\alpha_{s_a}$.

The actual case finds Q_L due to both radiation and conduction, modified by cover and base surface degradation. The net effect is to approximate the radiation-dependent case. This is borne out by temperatures observed during tests in the space simulator when the solar simulation intensity was varied by a factor of 2.6. Therefore, Eq. (6) was used in calculating the degradation of the sample surfaces.

a. Black. The cruise data for the black sample are plotted in Fig. 16. The sample ran cooler than the nominal sample predictions. This fact is attributed to the large (145°F estimated) differential between the sample and the base. The data were very consistent with the decrease in temperature expected with the increasing distance from the Sun. The switching events, once the wiring error was recognized, were predictable to within 8 hr of the actual times until February 13, at which time a very premature step of thermometer 4 occurred. The data from the 7 steps observed for the first three thermometers verified the preflight prediction of little degradation of the paint and gave confidence in the operation of the temperature sensor system.

The premature first step of thermometer 4 has been attributed to a design oversight not affecting the data of the other three thermometers. As mentioned before, the thermometers are resistant to 100-g accelerations as long as the mercury meniscus has not advanced into the gas chamber or receded into the Mercury chamber. During the midcourse maneuver, the black sample temperatures remained above 235.1°F, well above the 179.9°F top switching point of thermometer 4. At this elevated sample temperature, the mercury would be welling up into the gas chamber where, apparently, it was vulnerable to the shock of the pyrotechnic midcourse motor valves and the lateral 0.1-g midcourse correction acceleration. The result was the separation of a ball of mercury from the mercury thread in the gas chamber with a consequent approximate 25°F increase in the switching temperature. The accelerations experienced after the separation were insufficient to reunite the ball with the main mass of mercury. The subsequent performance

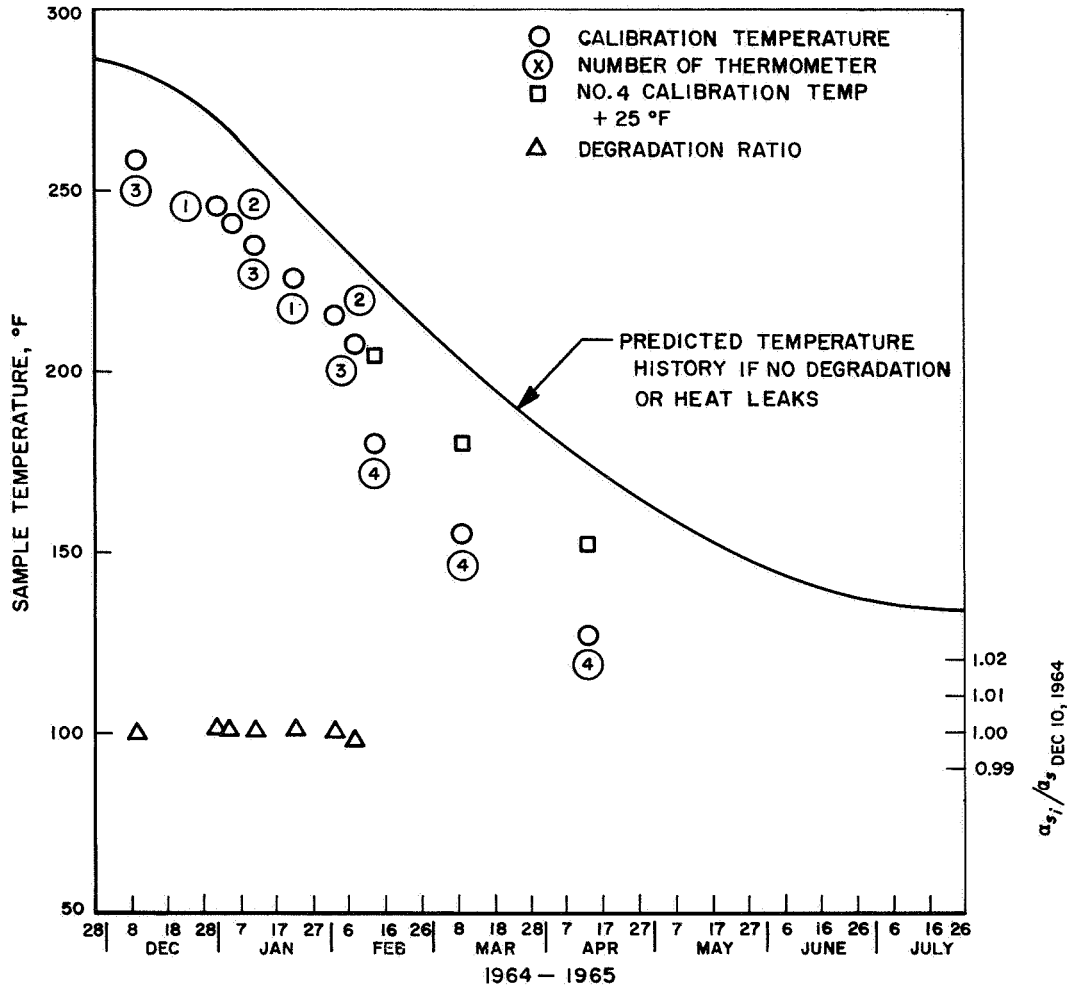

Fig. 16. Cruise mode data for black sample

of thermometer 4 was more difficult to predict to within closer than about 30 hr.

The degradation curve of the black sample is quite flat, showing that the surface properties do not change significantly in space.

b. ARF-2 white paint. The cruise mode data are plotted in Fig. 17, indicating continuing degradation of the sample. Initially, the sample temperature rose, showing that the degradation was progressing more rapidly than the decrease in solar intensity. Later, the Sun–spacecraft distance increased rapidly enough that the sample temperature fell below the initial switching temperature on January 6, 1965. After that time, the data showed a consistent rate of degradation so that the data curve, which started above the nominal curve, diverged from the latter. The final data point is interesting, as it was the only step that occurred after aphelion and before spacecraft telemetry turnoff.

The ARF-2 sample has a black control stripe to raise the sample temperature at Mars above the freezing point of mercury. Since the black paint showed negligible degradation, its solar inputs to the sample can be subtracted and the degradation of the ARF-2 can be determined. The $\alpha_{s_i}/\alpha_{s_0}$ information is plotted on a log format in Fig. 18, to provide a rate of degradation over the entire mission. It was found that the degradation was proceeding at a rate about 10 times as high as was measured in the UV exposure tests at the Illinois Institute of Technology Research Institute (IITRI) leading to the selection of the sample. The $(\alpha_s A_p)$ of the black control stripe is approximately twice the $(\alpha_s A_p)$ of the ARF-2

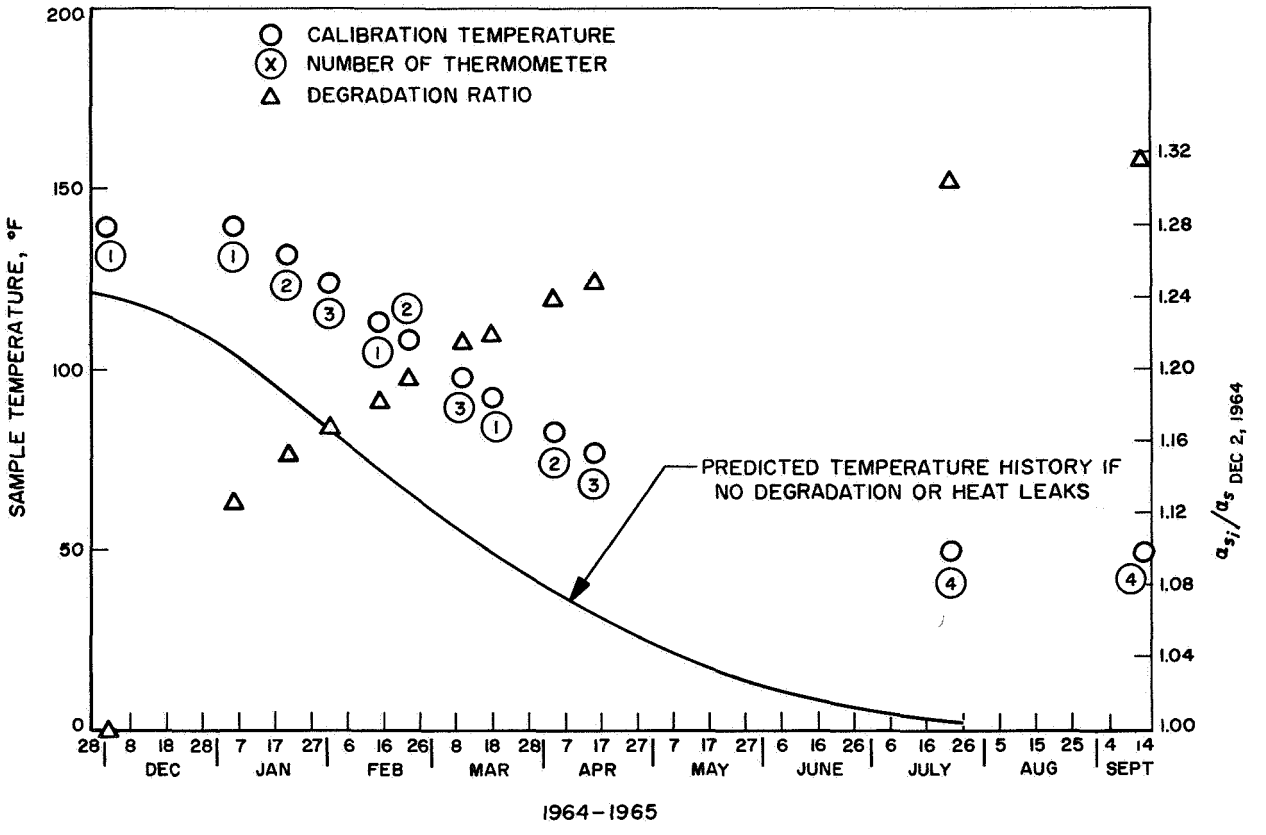

Fig. 17. Cruise mode data for ARF-2 white paint sample

paint so that any degradation of the black paint would greatly influence the interpretation of the ARF degradation. The lack of change of the surface properties of the black sample rules out any effect significant enough to greatly influence the curve.

The greater-than-predicted rate of degradation could be due to contamination of the sample surface in the space simulator, unexpected effects of space on the surface properties, or susceptibility of the particular paint batch to degradation. To determine the effect of the space simulator, the α_s of two samples painted at the same time as the flight hardware, one exposed to testing in the space simulator and the other as painted, was measured. The two samples were then exposed to a standard ultraviolet degradation test of 1000 Sun UV equivalent hours. The pre-test values of α_s were 0.16 to 0.17 for the fresh sample and 0.18 for the simulator exposed sample. While these two samples were being UV exposed, the relatively small change in surface properties caused by the simulator testing was examined and the theory of degradation caused by soft proton bombardment (1 kev) of the solar wind was advanced. The best available data of degradation effects from soft proton bombardment seemed to agree quite well with the flight data. This appeared to answer the question of why samples of ARF-2 in Earth orbit did not show this degradation since these samples would not see the solar wind. This theory would mean that current degradation qualification testing of white paints was invalid.

The results of the UV exposure tests were within 20% of the observed flight data, implying that the degradation was more associated with the paint, itself, than with the flight environment. There seemed to be a wide variation in the performance of different batches of ARF-2 paint, although all are prepared and applied according to a rigid specification. The flight ARF-2 paint was prepared and sprayed at JPL, rather than at IITRI. The samples were painted on a rainy day, perhaps with an effect on the water-base paint. The analysis was clouded considerably when the data from a UV test on two other samples, painted at the same time as the flight samples (one exposed to the space simulator) showed degradation

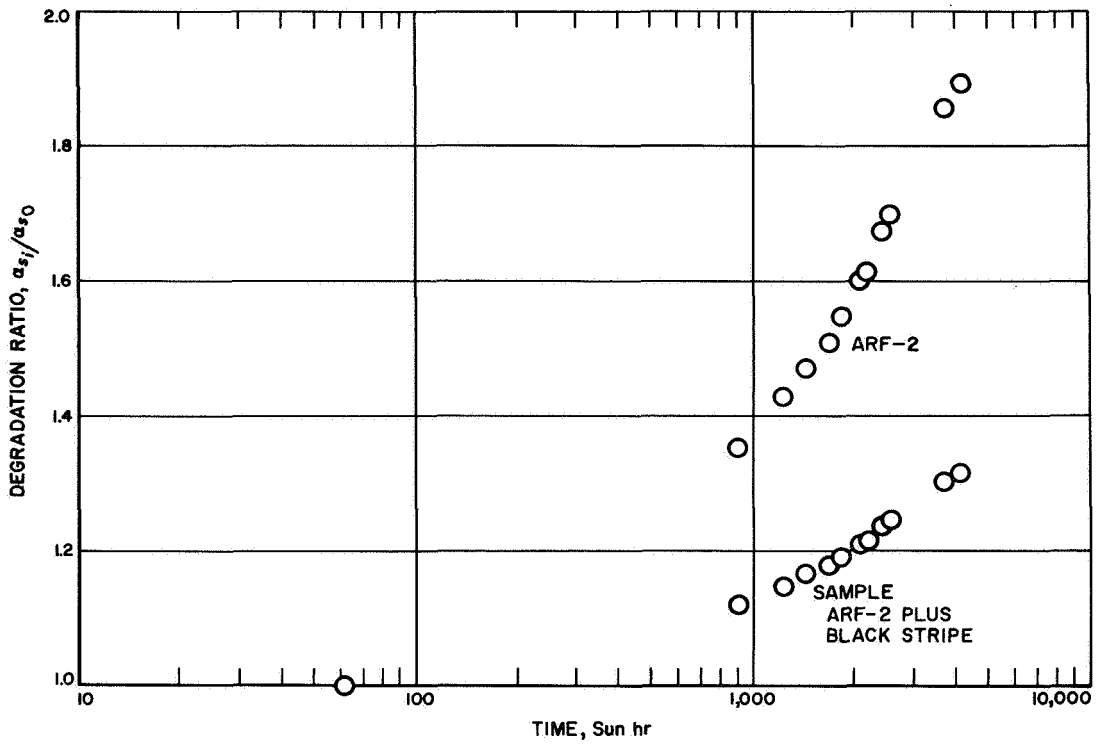

Fig. 18. Absorptance degradation of ARF-2 sample vs integrated flight exposure time

of a factor of 2 less than in the previous test. As before, the sample that had been exposed in the space simulator showed slightly more degradation than a virgin sample. As well as can be determined, the UV tests were identical with the same lamps and testing.

The ARF-2 sample did degrade significantly in space, but currently, the reasons are not fully understood.

c. Polished aluminum. The cruise data for the polished aluminum sample are plotted in Fig. 19. The sample exhibited an increase in temperature shortly after launch, similar to the white sample. The temperature passed back through the initial switching temperature 45 days later. The polished aluminum surface was not expected to have a change in surface properties in space. Therefore, by assuming that the degradation of the sample is due solely to yellowing of the ARF-2 stripe, it is found that the stripe degraded 35% more than the ARF-2 on the white sample during this 45-day period. When the channel 433 data are plotted as temperature vs time, using the flight calibration temperatures, an inconsistency is noticed between the first two points (thermometer 1) and the remainder of the data. A downward 6°F shift of thermometer 1 calibration or a 6°F upward shift of thermometers 2 and 3 places the data in line. The $\alpha_{s_i}/\alpha_{s_0}$ for a polished aluminum sample with degradation due to just the ARF-2 stripe, based on the white sample data, is plotted in Fig. 19, passing through the January 15 $\alpha_{s_i}/\alpha_{s_0}$ point for the polished data. It is seen that when the thermometer 1 calibration is shifted downward 6°F, the data after January 15 roughly follow this prediction curve.

Two different hypotheses might be drawn from the data. The first is that something is wrong either with thermometer 1 or the sample surface. A properly placed gas bubble in the thermometer mercury thread could cause the channel signal first to decrease 6 *dn* and later increase back to 28 *dn* as the sample cooled. This theory is not supported by the data seen during the transient period following launch when all sensor steps were in the proper sequence and of nominal value. A gas bubble in the mercury bulb would lower the switching temperature and would slow the mercury meniscus response to temperature changes, since the gas bubble would partially compensate for changes in the mercury volume. This would not explain the extended period between the first two steps, because the mercury meniscus would still be at a specific point for a given temperature. A chip of ARF-2 raising up from the sample cylinder early in the flight would cause a step function rise in the sample temperature. If the chip remained attached to adjacent paint, 14% of the ARF-2 paint separating would be sufficient. Such a chip is 0.2 in. square.

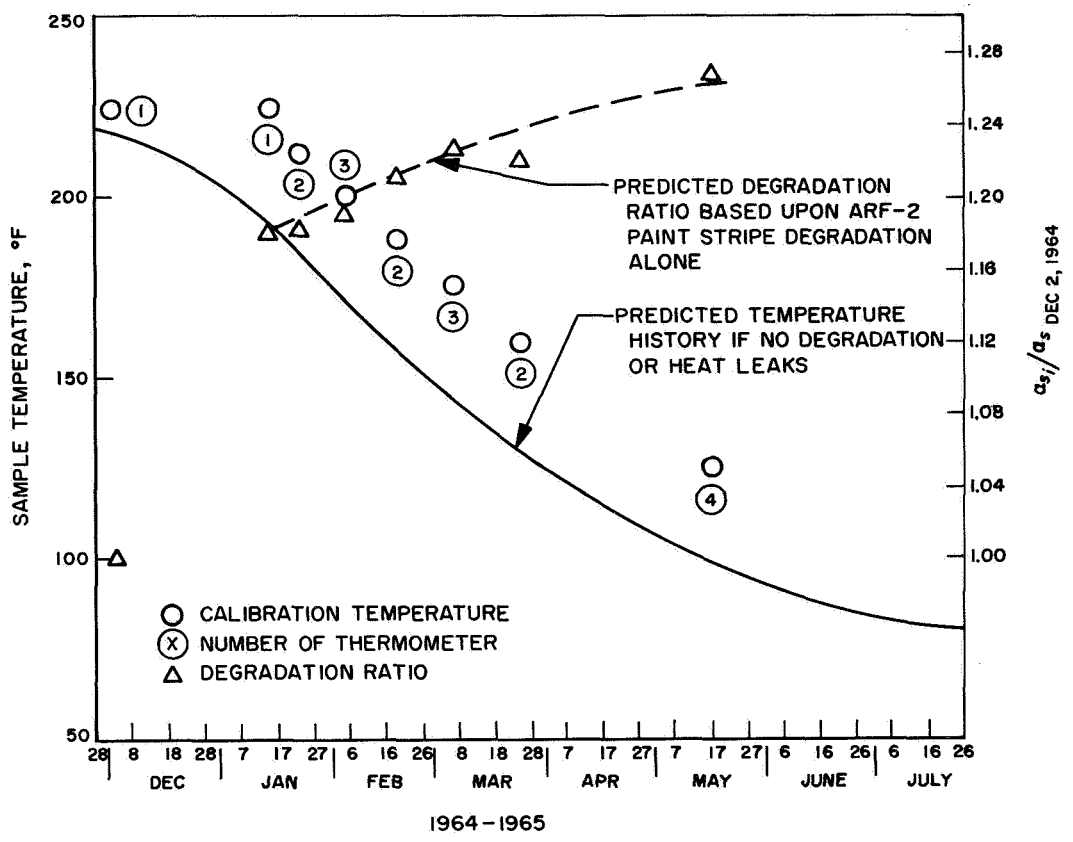

Fig. 19. *Cruise mode data for polished aluminum sample*

The second hypothesis is that the data is valid. If the ARF-2 stripe degraded at the same rate as the ARF-2 on the white sample, then the α/ε ratio of the polished aluminum must have changed early in the flight and was constant thereafter. This could be explained by a cleaning of the polished surface by the hard vacuum of space. A decrease in ε from 0.05 to 0.025 would be sufficient to account for the observed change in α_s beyond that attributable to degradation of the ARF-2 stripe.

Unfortunately, the initial space equilibrium temperature was such that only the lowest step on thermometer 1 was seen. Had two different temperature steps been observed, the reason for the data characteristics would be more easily isolated.

The polished aluminum sample has two Problem/Failure Reports (PFRs) written against it. The 152.4°F (final step of thermometer 3) step was completely absent. The reason has not been isolated concretely but seems most likely a broken thermometer leaking mercury that shorted out the resistor used for indicating this temperature. During the transient following launch, the sensor stepped properly, with the nominal sequence observed. The missing 152.4°F step was then present. Following this time at which the advancing thermometer mercury thread shorted out this resistor in the normal manner, an external short would have had to occur, preventing the 152.4°F step in the cruise data.

The second PFR was written when the step subsequent to the missing 152.4°F occurred two weeks early. The reason for this is felt to be the same as the reason for the black sample sensor calibration being changed. The 125.4°F top switching temperature of thermometer 4 is well below the 220°F minimum temperature at the time of the midcourse maneuver. Therefore, mercury could be welling up into the gas chamber, and the thermometer would be vulnerable to accelerations.

The data for the polished aluminum sample showed that, generally, the polished metallic surface is not affected by space and solar radiation, except for a period immediately after launch. Unfortunately, the ARF-2 stripe dominated the sample emissivity and masked all but gross changes in the α_s of the polished aluminum. An uncertainty in the early data prevents determination of the degradation of the polished surface during that period.

d. Aluminum silicone. The flight cruise data are plotted in Fig. 20. The aluminum silicone paint shows degradation of the surface properties with time at a rate greater than predicted. The data is somewhat hard to interpret, as there is evidence of calibration shifts. Because the sample temperature started rather low in the sensor range, only one step was seen on each of two thermometers, thereby reducing the chance to determine the amount of shifts in calibration. As a result, it is difficult to pinpoint the individual temperature precisely, but the degradation rate is decipherable since a calibration shift has only a small effect.

Correlating the two steps on thermometer 3 with the three steps on thermometer 4, it appears that the latter's calibrations have shifted 4°F upward relative to the former, probably arising from similar reasons as the black sensor shift, but of smaller magnitude since the sample was not as warm at midcourse. Thermometers 1 and 2 read 1.8°F and 4.6°F higher, respectively, when compared with thermometer 3.

This channel did not switch until the 38th day of flight. The minimum degradation occurring during this period can be estimated by the maximum temperature the sample could be without another step having occurred. To not have had another data point on thermometer 2, at least a 7.4% change in α/ε is required from launch until the first step is seen. The degradation curve plotted in Fig. 20 includes the 7.4% minimum value.

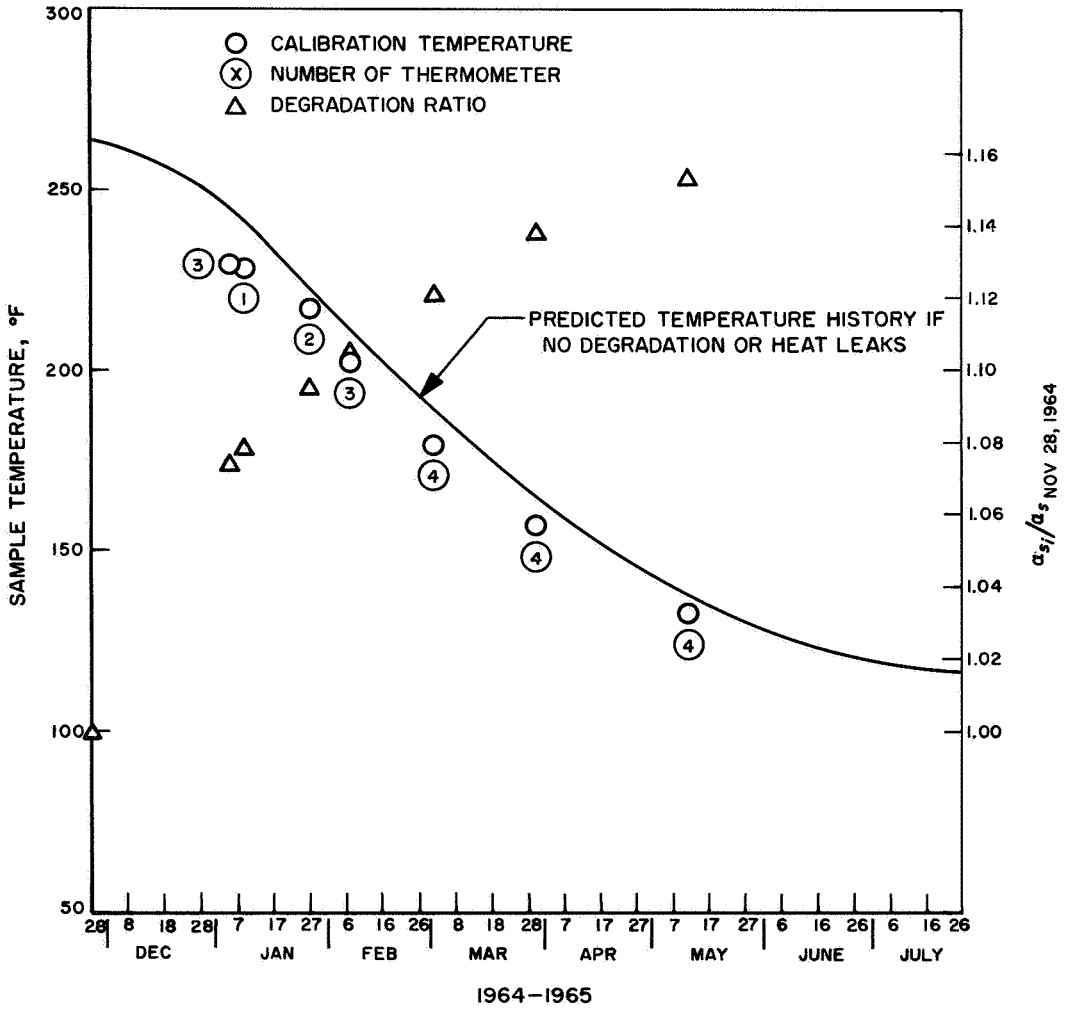

Fig. 20. Cruise mode data for aluminum silicone paint sample

VI. COMPARISON OF FLIGHT AND SPACE SIMULATOR DATA

The gray, or flat, spectral response of the black and aluminum silicone paints permits these two samples to serve as a comparison between the solar and solar-simulation intensities. Reduction of the flight and simulator test data revealed that the near-Earth solar simulation intensity was 10 to 11% greater than the facility instrumentation indicated. As noted in the discussion on the various tests run in the space simulator, there were great differences in temperatures between certain tests (Table 2), which would indicate that the error in intensity was not consistent. Subsequent evaluation tests of the chamber have verified an error either in the calibration or in the use of the instrumentation of the solar simulator.

The absorptance of the ARF-2 and polished aluminum surfaces to the mercury xenon solar simulation was computed with the assumption that the simulation intensity was 10% high. It was found that the α of ARF-2 in the simulator is 37% greater than in space. Similarly, the α of polished aluminum is 9% higher in the simulator than in true sunlight, which can be compared with 52 and 10% for the ARF-2 and polished aluminum, respectively, based on the best laboratory estimates for α in a mercury-xenon arc source.

The comparison is valid, since the samples are the same in both the simulator tests and flight, and any instrument errors would be duplicated in both environments.

VII. CONCLUSIONS

The heat losses of the samples to the base and covers have proven to be larger than anticipated. Therefore, the inflight measurements of α_s are less accurate than desired. Rather than verifying the laboratory α_s predictions, the laboratory values have been used to compute instrument errors. These losses were masked during environmental chamber tests by faulty solar simulation intensities raising the sample temperatures to the low-loss levels.

The determination of the degradation rates of surfaces due to space effects was not seriously affected by the sample heat losses since these are related to the absorptivity standard component temperatures and, therefore, are Sun dependent, as are the sample temperatures.

The absorptivity standard did show that spectral mismatch of the solar simulation to sunlight will affect the temperatures of such non-gray surfaces as ARF-2 white paint and polished aluminum.

The sample selection was reasonable. The black paint, as expected, did not degrade significantly and aided in evaluating the space simulator. The ARF-2 white paint showed the UV qualification based on a single batch, alone, may not be valid, confirming a *Mariner* philosophy to avoid flying a white paint in sunlight if possible. As a result of the flight data, further testing of ARF-2 samples painted at the same time as the flight sample surface is underway.

The aluminum silicone sample showed degradation, although the degree is open to question. The polished aluminum sample gave an indication that, perhaps, it vacuum-cleans during the first days of flight. Beyond that point, the surface seemed stable. Unfortunately, the ARF-2 stripe dominated the sample emissivity and masked all but gross changes in the α_s of the polished aluminum.

The temperature measurement system is basically sound, but design details resulted in problems during the fabrication of the sensors and during the midcourse maneuver. A modification of the thermometers to include a longer capillary above the top switch point would eliminate this failing. A system of resistance thermometers calibrated by digital thermometers would be an improvement, since a continuous record would be received and thermocouples would not be required for the simulator tests.

The hardware has shown some deficiencies, although the principles are good. The conduction and radiation

coupling of the sample to the cover and the base should be reduced. Similarly, the sample size should be increased to reduce the effects of any losses. A subsequent design, incorporating these features, has been built at JPL to demonstrate these improvements.

Although less than optimum as an engineering experiment, because of both real and imaginary constraints, the absorptivity standard has provided a significant addition to what little is known about the behavior of temperature control surfaces in interplanetary space.

VIII. RECOMMENDATIONS

It is recommended that further experiments relating to space effects on surface properties be flown. Importantly, in the *Mariner IV* investigation, knowledge of how to construct a flight instrument for such a purpose has been gained, and it has been demonstrated that an engineering experiment of modest proportions can return valuable information. The value of information to be secured from a future absorptivity standard instrument should be emphasized to secure a higher spacecraft priority and minimize the constraints on power, weight, size, and location on the spacecraft.

To investigate the effects of various space environment factors, an improved design would include larger and, perhaps, increased numbers of samples that are more completely isolated from conduction and radiation losses. Redesign could improve the function in several ways: prevent solar radiation from bypassing the sample surface and heating other areas of the sample assembly; counteract the uncertainties in radiation view factors back to space (caused by the sample cover overhang); incorporate a resistance thermometer that would give a continuous temperature readout calibrated by stepping mercury thermometers; and modify the mercury thermometer design to give vibration resistance over a wider band of temperatures.

It is further recommended that the effects of ground variables be investigated more thoroughly, that tests of UV degradation be run on more than one batch of paint and should include samples made by the user, and that the effects of soft proton bombardment (of approx 1 kev) should be studied for possible contribution to degradation.

APPENDIX
Error Analysis

I. BASIC COMPUTATIONS

The thermal balance of a sample surface can be written as:

$$SA_p\alpha_s = \sigma\varepsilon A_t T_s^4 + Q_L \qquad \text{(A-1)}$$

where Q_L = conduction and radiation losses from sample cylinder

$$= \sum\left[k(T_s - T_e)\right] + \sum\left[\sigma\varepsilon A_t(T_s^4 - T_e^4)\right]$$

S = solar intensity, Btu/hr-ft^2

A_p = projected area of surface seeing solar radiation, ft^2

α_s = solar absorptance of surface (integrated with respect to wavelength)

σ = Stefan-Boltzmann constant 1.716×10^{-9} Btu/hr-ft^2 °R^4

ε = hemispherical emittance of surface

A_t = total effective radiating area, ft^2

T_s = temperature of the sample surface, °R

T_e = temperature of environment or adjacent item, °R

k = thermal conductivity, Btu/hr-ft °F

The flight parameter is T_s; those that are peculiar to the space environment are S, α_s, and ε. Although it would be desirable to determine the independent contribution of S, α_s, and ε, it can be concluded from Eq. (A-1) that this is not possible with a temperature measurement only. The apparent absorbed energy $S\alpha_s$, however, can be separated from ε by assuming that laboratory information on ε is valid in the space environment; this assumption is of value because it permits a more direct comparison of simulated with actual solar radiation and gives a better indication of the surface's absorptance. Similarly, S and α_s could be separated by using existing information about S; however, this assumption would be less valid because both S and α_s are strong functions of wavelength. The distribution of energy as a function of wavelength is uncertain for most of the arc sources used in solar simulators and, to a lesser extent, for the solar flux. In addition, α_s for some surfaces – particularly white paints – varies with exposure, such changes occurring in localized spectral bands.

The stability of ε under space conditions is open to speculation, since very little data (if any) are available to support this assumption. Laboratory experience tends to indicate that the emittance is a strong function of the microscopic structure of a surface, and that ε is unchanged unless the surface structure is damaged or contaminated.

The surface structures of many black paints are noticeably very fragile; however, the black epoxy paint selected for the *Mariner* flight hardens to a very durable surface. During one test in air with a mercury xenon solar simulator, oxidation of the black paint was noted; therefore, illumination by the solar simulation when the chamber was not pumped down was carefully avoided in the preflight tests. The surface of the white paint (ARF-2) is relatively fragile; while physical damage to the surface has a noticeable effect on α_s, the effect on ε is small. Also, emittance change from damage to the white paint is minimized because of the application of the ARF-2 paint over a primer coat of PV-100, which has about the same emittance and is much more durable.

The emittance of the polished aluminum surface and that of the aluminum silicone paint are more uncertain. The emittance of the polished metal can change noticeably with a deposit of a relatively small amount of oil; however, this contamination can be removed easily, either by manual cleaning or by vacuum heating. The latter could have occurred during the early days of the flight. Of more concern was a gross change in the emittance of the polished aluminum from an effect commonly known as *reactor varnish*, which can occur if a metallic surface is bombarded with low-energy protons

in the presence of a contaminant. This could possibly occur during flight if the outgassing products of the spacecraft materials provided the contaminants and the solar wind provided the proton flux. From the flight data, such a gross change in ε would have lowered the sample temperature noticeably — an effect that was not observed.

The aluminum silicone paint achieves its surface properties in a rather unique way. Flakes of metallic aluminum are floated in a silicone matrix in such a way that the stability of the emittance depends on two factors: (1) The thin layer of silicone matrix material over the metal flakes could degrade due to solar radiation. The ε effect would be small, although a noticeable increase in α_s would result. (2) The emissivity of the aluminum silicone paint depends on a number of small cavities formed by the randomly oriented flakes of aluminum in the matrix, which characteristic tends to make the emissivity of aluminum silicone paint vary with application. Since this variation would also be apparent in the laboratory measurements, it can be accounted for in the error analysis. Because the aluminum silicone paint is not a homogeneous material, it could be inadvertently damaged in an attempt to clean it. In such an event, the α_s, as with the white paint, would change considerably more than ε, and such would be easily noted in the flight data. Therefore, it is probable that the stability of ε is a good assumption for coatings selected for the absorptivity standard.

A worst-case error for the absorbed energy ($S\alpha_s$) can be derived by dividing both sides of Eq. (A-1) by A_p, differentiating and summing the partials.

$$d(S\alpha_s) = \left[\frac{\sigma A_t T_s^4}{A_p}\right] d\varepsilon + \left[\frac{\sigma \varepsilon T_s^4}{A_p}\right] dA_t + \left[\frac{4\sigma\varepsilon A_t T_s^3}{A_p}\right] dT_s$$

$$+ \left[\frac{\varepsilon A_t T_s^4}{A_p}\right] d\sigma + \left[\frac{1}{A_p}\right] dQ_L + \left[\frac{\sigma\varepsilon A_t T_s^4 + Q_L}{A_p^2}\right] dA_p \qquad \text{(A-2)}$$

Division of Eq. (A-2) by

$$S\alpha_s = \frac{\sigma\varepsilon A_t T_s^4 + Q_L}{A_p}$$

then approximation of the differentials by Δ's gives

$$\frac{\Delta(S\alpha_s)}{(S\alpha_s)} = \left[\frac{\Delta\varepsilon}{\varepsilon} + \frac{\Delta A_t}{A_t} + \frac{4\Delta T_s}{T_s} + \frac{\Delta\sigma}{\sigma}\right]\left[\frac{\sigma\varepsilon A_t T_s^4}{(\sigma\varepsilon A_t T_s^4) + Q_L}\right]$$

$$+ \left[1 - \frac{\sigma\varepsilon A_t T_s^4}{\sigma\varepsilon A_t T_s^4 + Q_L}\right]\left[\frac{\Delta Q_L}{Q_L}\right] + \frac{\Delta A_p}{A_p} \qquad \text{(A-3)}$$

where

$$\frac{\Delta (S\alpha_s)}{(S\alpha_s)} = \text{the uncertainty in the absorbed energy}$$

$$\left[\frac{\Delta\varepsilon}{\varepsilon} + \frac{\Delta A_t}{A_t} + \frac{4\Delta T_s}{T_s} + \frac{\Delta\sigma}{\sigma}\right] = \text{the uncertainty in radiated energy}$$

$$\left[\frac{(\sigma A_t \varepsilon T_s^4)}{(\sigma A_t \varepsilon T_s^4) + Q_L}\right] = \text{the fraction of the absorbed energy radiated to space}$$

$$\left[1 - \frac{\sigma\varepsilon A_t T_s^4}{\sigma\varepsilon A_t T_s^4 + Q_L}\right] = \text{the fraction of the absorbed energy lost from the sample via conduction and stray radiation}$$

$$\left[\frac{\Delta Q_L}{Q_L}\right] = \text{the uncertainty in the heat losses}$$

$$\left[\frac{\Delta A_p}{A_p}\right] = \text{the uncertainty in the projected area}$$

II. DISCUSSION OF INDIVIDUAL ERROR TERMS

A. Uncertainty in Emittance $\Delta\varepsilon/\varepsilon$

Laboratory measurements of ε are generally reproducible to within $\pm 1\%$, with either reflectance or calorimetric techniques. With surfaces having a relatively large ε, the surface property can also be reproduced within approximately $\pm 1\%$ from sample to sample. This is not true for the polished aluminum sample, however, because minor variations in the condition of the surface can result in variations in ε as great as $\pm 50\%$. Since ε is small for the aluminum surface, the amount of heat transferred via radiation from the polished surface is also small relative to the heat radiated from the white control stripe or lost by conduction. Therefore, the large uncertainty in ε of the polished surface will have little effect on the determination of $S\alpha_s$.

B. Uncertainty in Total Effective Radiating Area $\Delta A_t/A_t$

The diameter of the hole in the cover is measured to a 0.001-in. tolerance, resulting in a 0.2% error. The width of the control stripes on the white and the polished samples can be measured to within 0.002 in. Since the emissivity of black and white paints is very similar, a negligible error is introduced. The difference in emissivity between white paint and polished aluminum, combined with the accuracy of the stripe-width measurement, gives a 0.7% uncertainty.

The major uncertainty in A_t arises from the variable blockage of sample radiation to space by the cover. The cumulative tolerances in the components affect the spacing between the sample surface and cover, giving a range of view-factors to space from the sample of 0.866 to 0.772, with a nominal of 0.830, for an error of 4.3%.

C. Uncertainty in Temperature $\Delta T_s/T_s$

The temperature measurement accuracy depends on the temperature difference between the sample surface and the temperature transducer, the accuracy of the measurement of the transducer itself, and the accuracy of the interrogation of the transducer by the spacecraft. The differential between the sample and sensor temperatures is considered to be negligible. The sensor is almost completely surrounded by the aluminum sample cylinder, the thermometer mercury bulbs are at the end of the sensor most deeply immersed in the sample cylinder,

and any sensor heat leaks are from the end of the sensor opposite the mercury bulbs.

To provide better understanding of the errors in the sensor temperature measurement and interrogation, the spacecraft temperature transducer and two absorptivity standard sensor systems (a thermostat-switch system and a digital thermometer system) will be described.

1. Standard Temperature Measurement

Spacecraft temperature measurements are normally made by passing a 1-ma current through a resistance thermometer and measuring the voltage induced across the transducer. The voltage is converted into a data number (dn) in a 126-step digital format, and this number is relayed to Earth. By conversion from dn, the temperature of the transducer is then known to lie within a span of 1 to 1½°F.

The errors in the resistance thermometer, itself, arise from the calibration accuracy of 1% of the total range or 1.25°F and uncertainties of the resistance measurement of 0.1 Ω. Since the data encoder interrogation current is 1.000 ±0.005 ma, this would give a maximum variation in the indicated resistance of 3.0 Ω (600 Ω × 0.005 ma = 3 mv = 3 Ω), which corresponds to a temperature error of 3.7°F. The spacecraft does have a reference channel, channel 420, which is a precision temperature-compensated resistor of 550 Ω. With the assumption that this resistance is, indeed, constant, a variation in the 1-ma current of more than 0.0015 ma {[(0.8 mv)/dn]/550 Ω = 0.0015 ma} would change the channel 420 reading from 64 dn to 63 or 65 dn. Since the uncertainty is reduced to 1 dn, the error arising from current variations is 1°F.

The assumption that the data encoder resolution is 1 dn gives rise to another 1°F uncertainty. The data encoder of the *Mariner IV* had a better resolution than this, but at the time the absorptivity standard was designed, the data encoder specification called for 1-dn resolution. The assumption that the temperature measured falls at the center of the 1°F dn span gives rise to a 0.5°F uncertainty. The degree of commutation of the data encoder resulted in a given temperature transducer being interrogated between 14 and 168 min, depending on the data rate and mode. With a maximum temperature decrease of 1°F/day and the slowest data rate, the total temperature change in the 168 min is 0.12°F. A dn reading changed in mid-interval between readings gives a 0.06°F uncertainty.

The total error for a standard spacecraft temperature measurement is, therefore:

Sensor calibration	1.25
Sensor resistance	0.12
Data encoder current	1.00
Data encoder resolution	1.00
Data number span	0.50
Scan interval	0.06
Total	3.93, or ~ 3.9°F

If the reference channel 420 resistor were to fail, this total would jump to 6.7°F.

2. Thermostat-Switch Temperature Measurement

The platinum resistance thermometer with two thermostat-switches sensor system was designed to circumvent many of the above gray areas. Since the spacecraft systems generally do not vary much with time, inflight calibrations at the beginning and the end of the data period would permit inference of the spacecraft data collection system influences during the interim. The uncertainty would be a combination of the switch calibration, scan interval, and dn span. The thermostat-switches are calibrated to 0.25°F by use of the platinum resistance thermometers (with a calibration accuracy of 0.1°F) into which they are inserted. The scan interval again causes a 0.06°F uncertainty, and the dn span results in a 0.5°F tolerance. The total uncertainty is, therefore:

Thermostat-switch calibration	0.25
Scan interval	0.06
dn resolution	0.50
Total	0.81, or ~ 0.8°F

Although superior to the standard temperature measurement, the platinum thermometer and the thermostatic switches were not flown as part of the absorptivity standard. The bimetallic switches failed during prelaunch vibration testing. The mercury-in-glass digital thermometer described below was the design used during the actual flight.

3. Mercury-in-glass Digital Temperature Measurement

The digital thermometer system circumvents most of the interrogation system errors. Because the resistance

changes that signal a temperature cause at least a 6-dn signal variation, the digital sensor is insensitive to errors in the resistance measurement during calibration, fluctuations in the interrogation current, and uncertainties in the resolution of the digital format. The ±0.06°F resulting from the scan interval is unavoidable.

The individual thermometers were calibrated to ±0.05°F by the manufacturer. Following FA vibrational testing, switch points of the flight sensors were calibrated at the JPL Standards Laboratory to ±0.1°F accuracy, for both increasing and decreasing temperatures. The hysteresis at individual points was found to be 0.2 to 0.6°F, with a mean of 0.3°F. In general, this area of hysteresis did not include the manufacturer's calibration.

To check for hysteresis, an individual thermometer was tested by the Standards Laboratory. The hysteresis of two switch points was found to be 0.3 and 0.5°F with the specific switch temperatures, when heating and cooling, reproducible to 0.03°F. Since the rate of change of temperature during calibration was greater than the maximum rate seen in cruise, the transient flight temperatures should cause no uncertainties that are not included in the total calibration tolerance. The actual flight switching temperatures fall within the measured sensor hysteresis with a bias toward the lower limit, since the samples are cooling during the flight to Mars. The flight sensor calibrations were taken to be the average of the maximum cooling switch temperature and minimum warming switch temperature for a given thermometer step; alternately, it could be first decided whether the particular calibration spread is due solely to hysteresis or partially to too rapid a temperature change during calibration and, then, the degree of bias toward the lower limit estimated.

The calibration uncertainty is, therefore, 0.15°F for the hysteresis and 0.1°F for the calibration accuracy. The total uncertainty is:

Calibration hysteresis	0.15°F
Calibration accuracy	0.10
Scan interval	0.06
Total	0.31, or ~ 0.3°F

Relating the digital thermometer measurement uncertainty to a relative error in absolute temperature, the value is found to be 0.3/400 = 0.0006, or approximately 0.001.

D. Uncertainty in Stefan-Boltzmann Constant $\Delta\sigma/\sigma$

Experimental and theoretical values for the Stefan-Boltzmann constant differ by 1%, giving a maximum of ±0.5% variation of either value from their mean.

Reference back to Eq. (A-3) permits a typical uncertainty in the radiated energy for a sample to now be evaluated.

$$\left(\frac{\Delta\varepsilon}{\varepsilon}+\frac{\Delta A_t}{A_t}+\frac{4\Delta T_s}{T_s}+\frac{\Delta\sigma}{\sigma}\right)=\left[0.02+0.052+4(0.001)+0.005\right]=0.081 \qquad \text{(A-4)}$$

The second and third groups of terms to the right of Eq. (A-3) are the ratio of the heat radiated to space and the heat losses from the sample, to the absorbed energy expressed in terms that avoid the absorptance. They, however, require that the nominal value for radiated and lost heat be determined. It should be noted that these terms are not the same for the various samples, because of ε; nor are they constant during the flight, because of T_s.

The heat losses (Q_L) arise from variations of the sample from an insulated flat plate seeing just the sun and space. The combined effect of the upper thermal shield, the high-gain antenna, the low-gain antenna, and the boost dampers, is equivalent to a total form factor of 9% at temperatures similar to the temperature of the samples.

The major factor in the heat losses of the samples is in the guard and support system of the absorptivity standard, itself. A sample has radiation and conduction interchange with its cover and with the base, because of temperature differentials. Originally, the sunlit areas of the covers and the base were painted to reduce gradients, but materials considerations resulted in less-than-optimum coatings, so that large gradients are present, especially to the base.

Q_L, too, is of a different magnitude and relative importance for each sample, since the temperatures of the cover, base, and sample all vary, and the total heat absorbed and rejected by the sample is dependent on the surface properties. An uncertainty also exists regarding the specific cover and base temperatures because they were not monitored and the PV-100 white coating on the base is known to degrade with UV exposure. The conduction heat paths are from the sample cylinder into the support and through the cones to the cover and base, plus a parallel path through the wiring harness to the base. The radiation interchange is through the cavity between the sample cylinder and the support structure. In addition, there are radiation losses from the gap between the cover and the sample surface.

A calculation of these heat losses was made; the more significant losses are summarized in Table A-1. In these calculations, a heat balance for the sample, its supporting structure, and electrical connections was analyzed for the samples at 1 AU using the observed flight temperatures.

Table A-1. Heat losses based on the mathematical model

Computation	Sample losses, Btu/hr			
	White paint	Black paint	Aluminum silicone	Polished aluminum
Conduction losses to cover & base	0.189	0.226	0.182	0.159
Radiation losses to cover & base	0.315	0.666	0.502	0.435
Blockage of view of space	−0.205	−0.207	−0.066	−0.059
Radiation loss from sample-cover gap	0.066	0.177	0.185	0.185
Total computed model heat losses	0.361	0.822	0.803	0.720

From these values for Q_L and nominal values for the other parameters, the second and third terms of Eq. (A-3) can be evaluated for the same conditions.

$$\frac{\sigma\varepsilon A_t T_s^4}{\sigma\varepsilon A_t T_s^4 + Q_L} = \begin{cases} 0.803 \text{ for the white sample} \\ 0.789 \text{ for the black sample} \\ 0.516 \text{ for the aluminum silicone sample} \\ 0.500 \text{ for the polished aluminum sample} \end{cases} \tag{A-5}$$

and

$$1 - \frac{\sigma\varepsilon A_t T_s^4}{\sigma\varepsilon A_t T_s^4 + Q_L} = \begin{cases} 0.197 \text{ for the white sample} \\ 0.201 \text{ for the black sample} \\ 0.484 \text{ for the aluminum silicone sample} \\ 0.500 \text{ for the polished aluminum sample} \end{cases} \tag{A-6}$$

E. Uncertainty in Conduction and Radiation Losses $\Delta Q_L/Q_L$

Considering the difficulty in the determination of the heat losses, the uncertainties of Q_L must be relatively large. Possibly the most direct approach to determining the magnitude of $\Delta Q_L/Q_L$ is to assume that the surface properties of the black sample remain within laboratory measurement uncertainties at least during the initial portion of the flight. While it is a potentially poor practice to base an analysis on the data to be analyzed, an apparent stability of the black sample is suggested by the flight data. By use of the initial flight temperature for the calculation of the absorbed and radiated energy of the black sample, the losses (Q_L) can be derived from application of Kerchoff's law. Similarly, the uncertainty in the losses ($\Delta Q_L/Q_L$) can be calculated from the uncertainties in the absorbed and radiated energies. By rewriting Eq. (A-1), the heat losses from the sample can be expressed as:

$$Q_L = SA_p\alpha_s - \sigma\varepsilon A_t T_s^4 \tag{A-1a}$$

By differentiating and summing the partials

$$dQ_L = \left[(SA_p)\,d\alpha_s + (S\alpha_s)dA_p + (A_p\,\alpha_s)dS\right] - \left[(4\sigma\varepsilon A_t T_s^3)\,dT_s + (\sigma\varepsilon T_s^4)\,dA_t + (\sigma A_t T_s^4)\,d\varepsilon + (\varepsilon A_t T_s^4)\,d\sigma\right] \tag{A-7}$$

Division of Eq. (A-4) by Eq. (A-1a), approximation of the differentials by Δ's, and regrouping, is shown by Eq. (A-8):

$$\frac{\Delta Q_L}{Q_L} = \frac{SA_p\alpha_s\left(\frac{\Delta\alpha_s}{\alpha_s} + \frac{\Delta A_p}{A_p} + \frac{\Delta S}{S}\right) + \sigma\varepsilon A_t T_s^4\left(\frac{4\Delta T_s}{T_s} + \frac{\Delta A_t}{A_t} + \frac{\Delta\varepsilon}{\varepsilon} + \frac{\Delta\sigma}{\sigma}\right)}{SA_p\alpha_s - \sigma\varepsilon A_t T_s^4} \tag{A-8}$$

The solar input to the black sample ($SA_p\alpha_s$) calculated for a near-earth position is 3.498 Btu/hr, and the energy radiated to space from the sample ($\sigma\varepsilon A_t T_s^4$) is 3.064 Btu/hr. The uncertainty in the solar input depends on the uncertainties in α_s, A_p, and S.

F. Uncertainty in Surface Solar Absorptance $\Delta\alpha_s/\alpha_s$

The measurement uncertainty for α_s for the black is the same as that for ε, or $\pm 2\%$, since the same reflectance techniques are used. Actually the measured parameter is $(\rho\lambda)$ where ρ is the reflectance and λ is a small wavelength interval; α_s (or $1 - \rho$) is an integrated value over all wavelengths where there is significant solar flux. To avoid double bookkeeping, the uncertainty in the solar flux is included in the $\Delta S/S$ term.

G. Uncertainty in Projected Surface Area to Solar Radiation $\Delta A_p/A_p$

The diameter of the hole in the cover was measured to 0.001-in. accuracy, giving rise to a 0.2% uncertainty. It may be interesting to note for later reference that the control stripe affects the value of $\Delta A_p/A_p$ for the white sample. The width of the black stripe was measured to a 0.001-in. accuracy and was found to have a 0.002-in. variation, or an additional ½% uncertainty. The same effect is not apparent on the polished aluminum sample with the white stripe because the absorptance of the two surfaces are so nearly matched. Therefore,

$$\left(\frac{\Delta A_p}{A_p}\right)_{\text{black, al. sil., pol. al.}} = 0.002 \tag{A-9a}$$

$$\left(\frac{\Delta A_p}{A_p}\right)_{\text{white}} = 0.007 \tag{A-9b}$$

H. Uncertainty in Solar Intensity $\Delta S/S$

The uncertainty in the solar intensity stems from two sources – the value of the solar constant (the solar intensity at 1.0 astronomical unit, AU) and the position of the spacecraft in space. The latter uncertainty is negligible, but the value of the solar constant and its tolerance varies considerably among reputable sources. In no case is the uncertainty less than $\pm 2\%$; the more accepted value is $\pm 5\%$. For the purpose of this report a value of 2.00 $\pm 5\%$ cal/cm^2 will be used.

With these estimates, plus those listed in Eq. (A-4), the uncertainty in the heat losses from the black sample can be evaluated by substitution into Eq. (A-8).

$$\left(\frac{\Delta Q_L}{Q_L}\right)_{\text{black}} = \frac{3.498\,(0.02 + 0.02 + 0.05) + 3.064\,(0.074)}{3.498 - 3.064} = 1.248 \qquad \text{(A-10)}$$

III. SUMMARY OF ERROR ANALYSIS

A tabulation of the error sources discussed in the preceding paragraphs has been made in Table A-2. Possibly, the most striking observation from this summary is how great an error could occur if all of the individual uncertainties were additive. To compensate for this improbable condition, a root-sum-squared (rss) calculation has been included in parentheses in Table A-2 for comparison. Even so, uncertainty for the black and white samples is approximately 16% and the uncertainty for polished aluminum and aluminum silicone samples is about twice this value. The larger uncertainty in these latter two samples stems from the lower absorptance and/or emittance of the aluminum and aluminum-silicone surfaces, which results in a more unfavorable ratio of the heat losses to the energy absorbed and radiated.

For comparison with ground-based measurements, assume a ±5% uncertainty in the solar constant, another 2% for the spectral distribution of the energy, and a 3% variation in reflectance measurements of the samples. If these are added, a conservative estimate of the laboratory uncertainties (10%) is much smaller than those observed in flight. Therefore, the justification of the flight

Table A-2. Summary of error analysis

Error source	Term of Eq. (A-3)	White paint	Black paint	Aluminum silicone	Polished aluminum
A. Uncertainty in radiated energy Eq. (A-4)	$\left(\frac{\Delta\varepsilon}{\varepsilon} + \frac{\Delta A_t}{A_t} + \frac{4\Delta T_s}{T_s} + \frac{\Delta\sigma}{\sigma}\right)$	0.074 (0.050)[a]	0.074 (0.050)	0.074 (0.050)	0.081 (0.056)
B. Ratio of radiated to absorbed energy Eq. (A-5)	$\frac{\sigma\varepsilon A_t T_s^4}{\sigma\varepsilon A_t T_s^4 + Q_L}$	0.803	0.789	0.516	0.500
C. Ratio of losses to absorbed energy Eq. (A-6)	$1 - \frac{\sigma\varepsilon A_t T_s^4}{\sigma\varepsilon A_t T_s^4 + Q_L}$	0.197	0.201	0.484	0.500
D. Uncertainty in the heat losses Eq. (A-10)	$\frac{\Delta Q_L}{Q_L}$	1.25 0.698	1.25 0.698	1.25 0.698	1.25 0.698
E. Uncertainty in projected area Eq. (A-9)	$\frac{\Delta A_p}{A_p}$	0.007	0.002	0.002	0.002
Total uncertainty in the measurement of absorbed energy, Eq. (A-3) [Above error sources (A × B) + (C × D) + E]	$\frac{\Delta(S\alpha_s)}{S\alpha_s}$	0.313 (0.166)	0.312 (0.159)	0.645 (0.341)	0.668 (0.353)

[a]rss equivalent in ( ).

measurements does not lie in the inherent accuracy of the instrument, but in the exposure of the sample to a real, rather than a simulated, flight condition.

The error analysis is felt to be conservative although it is in some respects oversimplified and subjective. It should be noted that the uncertainty in $S\alpha_s$ not only varies from sample to sample, but will vary with time of flight. A portion of the heat losses are due to conduction to the base of the instrument and perhaps even to the upper ring of the spacecraft to which it is mounted. The surface of the base was painted with PV-100 white paint; degradation of this paint would reduce the temperature difference (hence, conduction losses) between the sample and the base. Another condition which would cause a variation in the conduction losses, though probably smaller, is the relatively constant temperature of the spacecraft compared with the changing temperature of the sample. From launch to encounter, an undegraded sample would drop about 125°F in temperature, while the spacecraft would drop only 30 to 35°F. Both the yellowing of the white base and the relatively constant spacecraft temperature reduce the conduction losses as the spacecraft approaches Mars. This effect is good in that the heat losses from the samples are reduced, but this reduction could be interpreted as an increase in heat input or a degradation of the sample surfaces.

There are two possible ways to identify this effect in the flight data. The degradation of the black and aluminum silicone samples should be small based on laboratory experience. If this is true in space, then the other two samples can be interpreted with reference to these samples. The more sensitive indicator of conduction losses (see Table A-1) would be the aluminum silicone sample. A second, more accurate, procedure would be possible if the spacecraft continued to transmit data when it began retracing its relative position with respect to the Sun. In such a case, the temperature distribution around the sample would be identical with that observed at the equivalent earlier point on the trajectory and any difference in the sample temperature would be an indicator of the α_s and ε of the sample (see Eq. A-1) limited only by the accuracy of the temperature measurement, or 0.4%. Fortunately, both of these conditions have occurred. Data are still being received from the spacecraft while it is retracing its temperature history, and these data indicate that both the black and aluminum silicone samples have experienced very little degradation.

To review this study of the error sources of the absorptivity standard, there are four principal indications:

1. An extremely accurate determination of the change in α_s and ε can be made as the spacecraft retraces its temperature history.
2. The uncertainty in the determination of $S\alpha_s$ using the absorptivity standard is large relative to standard laboratory techniques.
3. The accuracy of the data varies from sample to sample and with flight time.
4. The most significant source of uncertainty in the measurement of $S\alpha_s$ is in the determination of the heat losses from the sample.

REFERENCES

1. Johnson, F. S., "The Solar Constant," *J. Meteorol. II*, No. 6, December 1954.

2. Hickman, R. S., *Determination of Radiation Configuration Factors*, TR 32-154, Jet Propulsion Laboratory, California Institute of Technology, Pasadena, California, December 21, 1961.

ACKNOWLEDGMENTS

The authors wish to thank the following JPL personnel for their valuable contributions to this Report: James A. Brandt, who conceived the design of the absorptivity standard; James S. Brindley, who was responsible for the assembly and testing of the instrument; William F. Carroll, who assisted with the sample surface preparation and property measurements; and Hunter McConnell and James Stahnke of the JPL Standards Laboratory who calibrated the flight sensors. In addition, appreciation is expressed to Palmer Newbauer of Philadelphia Scientific Glass Co., and to Alan Loucks of WEMS, Inc. Finally, we are indebted to the *Mariner* Project Office for granting permission for the absorptivity standard instrument to fly aboard the *Mariner Mars* spacecraft.